A coupled extreme gradient boosting-MPA approach for estimating daily reference evapotranspiration

Mohammed Achite [a*], Hamid Nasiri [b,c], Okan Mert Katipoğlu [d], Mohammed Abdallah [e, f], Roozbeh Moazenzadeh [g], Babak Mohammadi [h]

[a] Faculty of Nature and Life Sciences, Laboratory of Water and Environment, Hassiba Benbouali University of Chlef, Chlef 02180, Algeria; m.achite@univ-chlef.dz
[b] School of Computing and Communications, Lancaster University, Lancaster, UK; h.nasiri@lancaster.ac.uk
[c] Department of Computer Engineering, Amirkabir University of Technology (Tehran Polytechnic), Tehran, Iran
[d] Department of Civil Engineering, Erzincan Binali Yıldırım University, Erzincan, Turkey; okatipoglu@erzincan.edu.tr
[e] College of Hydrology and Water Resources, Hohai University, Nanjing, Jiangsu 210024, China; m.abdallah.hhu@gmail.com
[f] The Hydraulics Research Station, PO Box 318, Wad Medani, Sudan
[g] Department of Water Engineering, Faculty of Agriculture, Shahrood University of Technology, Shahrood, Iran; romo_sci@shahroodut.ac.ir
[h] Independent researcher, Sweden; babakmsh@qq.com

*Corresponding author: Mohammed Achite (m.achite@univ-chlef.dz)

Abstract

Reference evapotranspiration (ET_0) modeling is pivotal for irrigation scheduling and water resources planning. This study presents a hybrid approach integrating Extreme Gradient Boosting (XGB) with Marine Predators Algorithm (MPA) for daily ET_0 estimation in northern Algeria. The proposed XGB-MPA model was evaluated against traditional empirical models and assessed using statistical methods. Shapley Additive Explanations (SHAP) was employed to enhance model interpretability. Various combinations of meteorological variables were tested as inputs, including air temperature, relative humidity, sunshine hours, wind speed, and extraterrestrial solar radiation. The XGB-MPA hybrid model achieved superior prediction

accuracy during testing (R^2 = 0.9958, RMSE = 0.1713 mm/day) compared to traditional empirical models and the standard XGB model. The study demonstrated that ET_0 prediction accuracy increased with the number of meteorological inputs used. Our findings highlight the XGB-MPA hybrid model's potential for accurate ET_0 estimation in northern Algeria, which can be used for water resource management and irrigation planning.

Keywords: Extreme Gradient Boosting; Hydroinformatics; Marine Predators Algorithm; Reference evapotranspiration; Shapley Additive Explanations.

1. **Introduction**

Reference evapotranspiration (ET_0) is an important parameter that reflects the combined impact of vegetation transpiration and soil evaporation over a given time period. Its estimation is closely associated with several meteorological variables like solar radiation, precipitation, wind speed, temperature, as well as other factors such as soil moisture and vegetation characteristics (Feng et al. 2016, Mehdizadeh et al. 2017, Ferreira et al. 2019). Accurate ET_0 estimation is crucial for the agricultural water management, prediction of crop yield, irrigation systems design, hydrological modeling, and agrometeorological studies (Gocic et al. 2016, Mystakidis et al. 2016).

The two processes that make up the ET_0 are crop transpiration into the atmosphere and soil evaporation (Chen et al. 2020). The energy and water cycles between the ground and atmosphere depend on ET (Hadria et al. 2021). Although various approaches have been employed to measure ET_0, such as the vorticity correlation approach, isotope tracer method, liquid flow method, and lysimeter method, they are usually laborious, time-consuming, costly, and difficult to handle across vast areas (Jiang et al. 2020). As a result, a number of ET_0 calculation models have been

proposed, with ET_0 serving as a key prerequisite for these models (Chen et al. 2020). For these models, it's essential to calculate ET_0 precisely and quickly.

Various statistical approaches have been investigated worldwide to estimate ET_0 (Temesgen et al. 2005, Azzam et al. 2023), but the Food and Agricultural Organization of the United Nations (FAO) considers the FAO56 Penman Monteith equation (FAO56-PM) as the sole benchmark mathematical approach (Pereira et al. 2015). This method has been demonstrated to be a highly accurate approach in a variety of climatic conditions (Espadafor et al. 2011, Cordova et al. 2015, Xu et al. 2018, Zhao et al. 2019). The FAO56-PM equation is dependent on several key meteorological parameters which may not be obtainable for a particular location, especially in developing countries, or their calculation is tedious and complicated (Moazenzadeh &Izady 2022). Consequently, the application of the FAO56-PM model can be significantly constrained in such areas. Thus, developing models for accurate ET_0 estimation with fewer meteorological variables is essentially required.

Accordingly, researchers have developed empirical approaches that need fewer input meteorological variables for ET_0 calculation. These approaches can be categorized into seven types (Zhang et al. 2018, Chen et al. 2020): (1) combination approaches, (2) radiation-based approaches, (3) temperature-based approaches, (4) humidity-based approaches, (5) water budget-based approaches, (6) mass transfer-based approaches, and (7) pan-based approaches. The most commonly approaches were extensively used are combination approaches, radiation-based approaches, and temperature-based approaches, whereas have been applied in many studies across different climate zones (Feng et al. 2017b, Reis et al. 2019, Valle et al. 2020, Adnan et al. 2021, Bellido-Jimenez et al. 2021). Valle et al. (2020) compared the performance of 21 empirical approaches for estimation daily ET_0 across the tropical semi-humid region in the Brazilian

76 savanna. They resulted that the radiation-based approaches were more accurate than the mass
77 transfer-based and temperature-based approaches. Yang et al. (2021) employed 18 different
78 empirical approaches to calculate daily ET_0 across different climate zones in China. They found
79 that the combination approaches had the best performance, followed by the radiation-based
80 approaches, while the temperature-based approaches performed the worst.

81 Machine Learning (ML) models have recently been utilized successfully for simulation various
82 hydrological and meteorological variables (Rezaie-Balf et al., 2021; Sun et al., 2021; Zhao et al.,
83 2021). These models are effective tools in ET_0 estimation because they have high capabilities to
84 capture nonlinear relationship between input and target variables (Ferreira &da Cunha 2020).
85 Various ML models have been studied, such as support vector machine (SVM) (Zhang et al. 2018,
86 Mohammadi &Mehdizadeh 2020), artificial neural network (ANN) (Yassin et al. 2016, Jing et al.
87 2019, Gao et al. 2021), generalized regression neural network (GRNN) (Ladlani et al. 2012, Feng et
88 al. 2017a), adaptive neuro-fuzzy inference system (ANFIS) (Shiri et al. 2015, Keshtegar et al. 2018,
89 Alizamir et al. 2020), and extreme learning machine (ELM) (Abdullah et al. 2015, Feng et al. 2016).
90 Generally speaking, ML models outperform empirical approaches for estimating ET_0, achieving
91 greater results when using same input data (Feng et al. 2016, Mehdizadeh et al. 2017, Fan et al. 2019,
92 Reis et al. 2019, Mohammadi &Mehdizadeh 2020, Abdallah et al. 2022, Achite et al. 2022). When
93 employing ML approaches for modeling ET_0, selecting less expensive and time-consuming
94 procedures is crucial (Yamac &Todorovic 2020). In addition to these approaches, tree-based ML
95 models are becoming more and more popular because of their very rapid processing and
96 acceptable accuracy, such as random forest (RF) (Feng et al. 2017a, Salam &Islam 2020, Zhu et al.
97 2020), extreme gradient boosting (XGB) (Yu et al. 2020, Abdallah et al. 2022), light gradient

boosting machine (LightGBM) (Fan et al. 2019, Sarigol &Katipoglu 2023), and gradient boosting with categorial feature support (CatBoost) (Fan et al. 2018, Huang et al. 2019).

The XGB model was introduced by Chen et al. (2016) for the purpose of producing strong classification techniques. The XGB calculates model weights and superimposes all inadequate classifiers to create robust classifiers. As an outcome, the estimation error is considerably reduced, and a classification outcome with higher prediction accuracy is possible (Jia et al. 2019). According to optimal accuracy, model flexibility, and computational effectiveness, the XGB model was recommended for daily ET_0 estimation in different climatic zones of China (Fan et al. 2018). There are successful applications of XGB model for ET_0 estimation in various hydroclimatic domains (Fan et al. 2018, Fan et al. 2019, Wang et al. 2019, Ferreira &da Cunha 2020, Fan et al. 2021, Abdallah et al. 2022, Agrawal et al. 2022, Jayashree et al. 2023). The XGB model exhibited equivalent accuracy to SVM and ELM when using the limited input data and outperformed RF and M5Tree models in tropical and subtropical humid climate (Fan et al. 2018). The XGB model showed equivalent performance to SVM and ELM models when using a full combination of meteorological data in hyper-arid region (Abdallah et al. 2022). Given its acceptable reliability, stability, and relatively low computation expenses, the XGB model is thus appropriate for estimating daily ET_0 in data-limited regions.

The parameters of ML models have a large impact on the prediction accuracy of the developed models. When the input data are very complicated, particularly, adjusting the model parameters typically needs much effort and expert expertise (Yu et al. 2020). There are several research employing optimization algorithms to select the optimal parameters in order to increase the effectiveness of parameter modification of ML models. For instance, Han et al. (2019) optimize the parameters of XGB model with Bat Algorithm (BA) for estimating daily ET_0 in different

climate zone of China. Yu et al. (2020) developed a novel approach throughout optimizing the XGB model with Particle Swarm Optimization (PSO) algorithm to estimate daily ET_0 by using limited input data in the Solar Greenhouse. They concluded that the POS-XGB model could obtain the highest estimation performance. Hybridization of XGB with whale optimization algorithm (XGB-WOA) for estimating daily ET_0 in arid and humid regions was investigated by Yan et al. (2021). Additionally, there still exist challenges with hyperparameter tuning, and the optimal parameter of the XGB model for estimating daily ET_0 remains to be issued. Recently, the Marine Predators Algorithm (MPA) was yielded better than PSO, genetic algorithm (GA), and grey wolf optimization (GWO) when used to optimize the ANN approach for prediction streamflow (Ikram et al. 2022). The advantages of MPA can be summarized as; (*i*) having fewer parameters, simple setting, easy to implement. MPA memorizes optimization results. It requires less iteration (Abd Elminaam et al. 2021). (*ii*) Another advantage of MPA is that it mimics predators' behaviors to increase the probability of escaping from local optima (Abdel-Basset et al. 2021). (*iii*) The MPA has shown fast convergence rates compared to other optimization algorithms (Al-Betar et al. 2023). (*iv*)The MPA is designed to search for the global optimum in complex and multimodal optimization problems (Faramarzi et al. 2020).

Since the ET_0 has significant spatial and temporal variations, further works in new stations appear to be necessary, with the goal of correct irrigation planning and control and management of water resource consumption, despite the availability of previous studies. Accordingly, it appears that it is important to conduct targeted studies in two areas. The first is related to the parameters, so that the most effective climatic parameters are used. The point here is that in many developing countries, such as Algeria, the input parameters of empirical ET_0 estimator models may be missing (not measured) or their accuracy may be questionable. On the other

144 hand, the existing empirical models have been developed for particular regions and may lead to
145 unreliable results in other areas. This has been confirmed even after the calibration of empirical
146 models in various studies (Ferreira et al. 2019, Nourani et al. 2019, Chen et al. 2020). Climate
147 change, which has gained momentum in recent years, can also affect ET_0 estimation by
148 influencing the changes in the range of variability of parameters, changes in the boundary values
149 of parameters, and displacement in the trends of parameter variations. Therefore, revisiting the
150 boundary values and the trend of variations of climatic parameters under the influence of climate
151 change is an important point that should be considered in future studies.

152 The second part pertains to ET_0 estimator models, which have made significant progress in
153 recent years. Artificial intelligence models with a better ability to model non-linear relationships
154 and to recover extrema have played an important role in this progress. Bio-inspired algorithms
155 have also played an important part in improving ET_0 estimation by optimizing the parameters of
156 base models (e Lucas et al. 2020, Maroufpoor et al. 2020). However, these algorithms may lead to
157 different results in different regions, and this highlights the importance of evaluating such
158 algorithms in various stations. Beyond the above-mentioned points, it appears that generalization
159 of ET_0 estimator models to regions other than those whose data have been used in model training
160 will be a key and major step toward developing models which can be used on a large (global)
161 scale. For this purpose, application of dimensionless meteorological parameters, similar to what
162 has been reported for the modeling of the solar radiation process (Mohammadi &Moazenzadeh
163 2021) can be fruitful.

164 Estimating ET_0 accurately in regions with limited meteorological data, such as northern Algeria,
165 presents unique challenges. Traditional empirical models, like the FAO56-PM, rely on extensive
166 meteorological inputs, often unavailable or unreliable in developing regions. This lack of data

constrains the applicability of such models and can lead to inaccuracies, especially in semi-arid environments where precise water resource management is critical. Moreover, traditional models may lack the flexibility to adapt to complex climatic conditions and the increasing variability brought by climate change. ML methods, particularly when combined with optimization algorithms, have shown promise in addressing these limitations by improving model accuracy with fewer inputs and enhancing adaptability across diverse environments. However, these models require optimized parameter tuning to achieve reliable results.

To address these challenges, this study introduces a novel hybrid ET_0 estimation model that combines the accuracy of XGB with the MPA for optimized hyperparameter tuning. By integrating these techniques, we aim to develop a model that not only improves ET_0 prediction accuracy in the data-limited, semi-arid Wadi Sly basin but also contributes a versatile and scalable approach that can be adapted to similar regions. This research ultimately supports sustainable water resource management by enabling more efficient irrigation planning and better-informed decision-making in regions facing water scarcity.

2. **Materials and methods**

2.1. **Study area**

As shown in Figure 1, the study area is the Wadi Sly basin, which is located in northwest of Algeria. It has an area of 1225 km^2, with coordinates of 35°36'5" - 36°5'53" N and 1°8'16" - 1°44'56" E. The basin has a maximum width and length of 30 and 70 kilometers, respectively. Besides, it has a narrow and long-form as well as a large hydrographic network. The Sidi Yakoub dam, which was built for agricultural purposes, influences flows in the lower section of the basin.

Northern Algeria represents a unique Mediterranean climate zone characterized by distinct seasonal patterns, with annual rainfall varying between 200-800 mm and significant spatial variability influenced by complex topographical features and coastal proximity. This region faces critical water management challenges due to its semi-arid characteristics, where agriculture consumes approximately 70% of available water resources while supporting a growing population of over 25 million inhabitants. The area experiences intense solar radiation and high evaporation rates, particularly during summer months when temperatures regularly exceed 35°C, making accurate ET_0 estimation crucial for agricultural sustainability. The region's agricultural sector, dominated by cereal cultivation and increasingly moving towards irrigated farming, faces mounting pressure from climate variability, urbanization, and groundwater depletion. These challenges are exacerbated by the intersection of traditional farming practices with modern irrigation requirements, creating a pressing need for precise ET_0 modeling to optimize water resource allocation. The region's unique combination of Mediterranean climate influences, varying topography from coastal areas to inland plateaus, and diverse agricultural practices makes it an ideal case study for advancing ET_0 prediction methodologies (Tadlaoui, 2018; Chetioui, and Bouregaa, 2024).

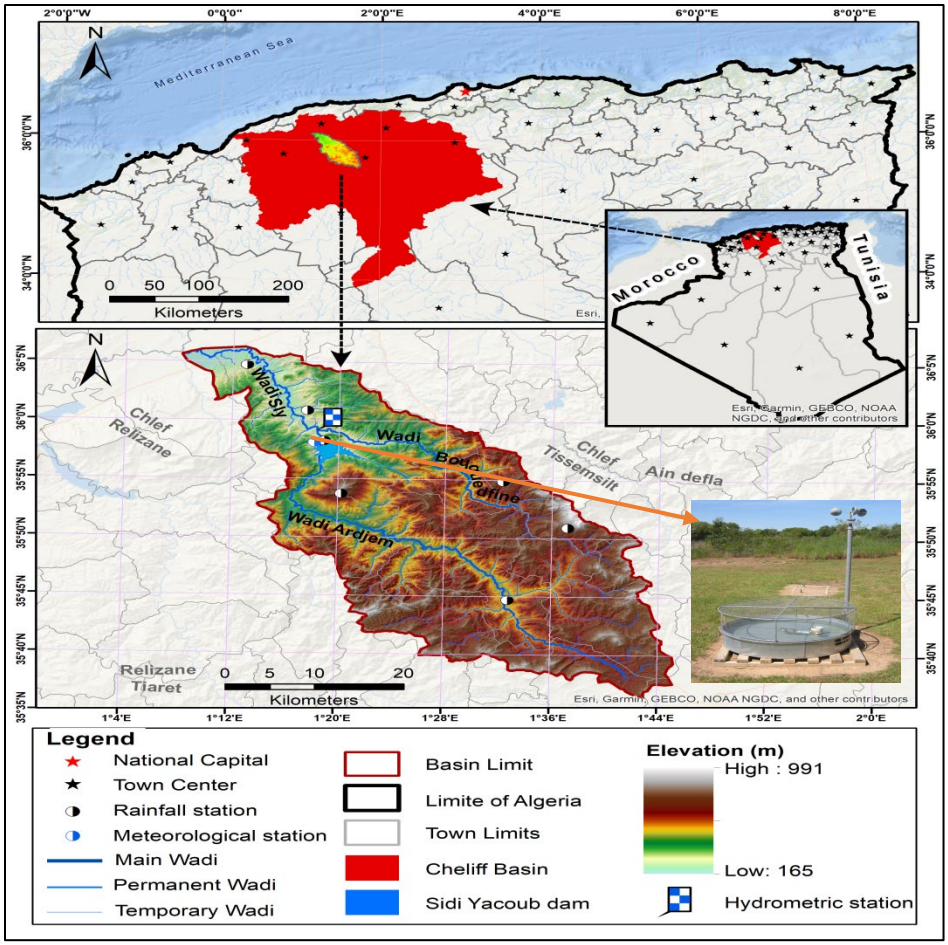

206

207 **Figure 1.** Location of the study area and the meteorological station

208

209

210

211 2.2. **Data collection**

212 The daily meteorological variables, including air temperature (Tmin, Tmax, and Tmean), relative
213 humidity (RHmin, RHmax, and RHmean), wind speed (U_2), sunshine hours (SSH), and pan
214 evaporation (Epan) were collected from the Sidi Yakoub meteorological station. The dataset

215 comprises daily records for 11 years from January 2000 to December 2010. Table 1 shows the
216 statistical characteristics for all data, training, and testing sets.

217 **Table 1.** Statistical measures of the meteorological data for all, train, and test datasets

Period	Variable	Mean	Standard deviation	Median	Minimum	Maximum	Range	Skewness coefficient	Kurtosis
All data	Tmean (°C)	20.19	7.49	19.38	3.35	40.15	36.8	0.2	-1.05
	Tmax (°C)	25.82	9.05	25	6.3	47.4	41.1	0.18	-1.08
	Tmin (°C)	14.57	6.27	13.9	0.1	33.3	33.2	0.18	-0.9
	SSH	8	3.79	8.8	0	14.2	14.2	-0.58	-0.67
	U2 (m/s)	2.83	1.41	2.6	0	11.4	11.4	1.19	2.92
	RHmean (%)	53.93	13.88	54.38	30	89.5	59.5	0	-0.95
	RHmax (%)	71.83	12.23	74.5	33	99	66	-0.62	-0.5
	RHmin (%)	36.03	17.42	34	2.5	87.5	85	0.33	-0.77
	Ra (MJ/m^2/day)	29.64	9.16	30.44	16.03	41.72	25.68	-0.13	-1.5
	Epan (mm/day)	7.63	5.11	6.55	0.1	23	22.9	0.48	-0.82
	ET (mm/day)	4.58	2.66	4.04	0.59	13.77	13.18	0.5	-0.78
Train data	Tmean (°C)	20.37	7.62	19.75	3.35	40.15	36.8	0.15	-1.12
	Tmax (°C)	26.02	9.16	25.2	6.3	47.1	40.8	0.12	-1.15
	Tmin (°C)	14.73	6.42	14.2	0.1	33.3	33.2	0.13	-0.95
	SSH	7.95	3.76	8.8	0	14.2	14.2	-0.56	-0.64
	U2 (m/s)	2.75	1.24	2.6	0	9.9	9.9	0.93	2
	RHmean (%)	52.86	13.89	53	30	89.5	59.5	0.07	-0.93
	RHmax (%)	70.63	12.28	73	33	99	66	-0.54	-0.62
	RHmin (%)	35.1	17.35	33	2.5	87.5	85	0.39	-0.71
	Ra (MJ/m^2/day)	29.64	9.16	30.44	16.03	41.72	25.68	-0.13	-1.5
	Epan (mm/day)	7.74	5.08	7	0.1	23	22.9	0.48	-0.8
	ET (mm/day)	4.63	2.68	4.08	0.59	12.6	12.01	0.46	-0.89
Test data	Tmean (°C)	19.7	7.1	18.5	4.05	38.85	34.8	0.36	-0.79
	Tmax (°C)	25.28	8.74	24.4	7	47.4	40.4	0.34	-0.82
	Tmin (°C)	14.13	5.83	13.5	1.1	30.7	29.6	0.3	-0.71
	SSH	8.14	3.86	9.1	0	13.9	13.9	-0.61	-0.74
	U2 (m/s)	3.04	1.76	2.8	0	11.4	11.4	1.18	2.07
	RHmean (%)	56.79	13.45	58.5	30	87.75	57.75	-0.2	-0.88
	RHmax (%)	75.06	11.5	78.5	42.5	98	55.5	-0.87	0.01
	RHmin (%)	38.53	17.36	38.5	2.5	85	82.5	0.17	-0.86
	Ra (MJ/m^2/day)	29.64	9.17	30.44	16.03	41.72	25.68	-0.13	-1.51
	Epan (mm/day)	7.33	5.16	6.2	0.1	22.1	22	0.51	-0.88
	ET (mm/day)	4.45	2.58	3.95	0.63	13.77	13.14	0.63	-0.43

218

219 2.3. **Empirical approaches and measured pan evaporation**

For ET_0 time series estimation, eight empirical models were applied, including those based on temperature, mass transfer, radiation, and various meteorological data. As previously stated, the FAO-56 PM is regarded as a valid technique of estimating ET_0, therefore ET_0 values of FAO-56 PM were considered as benchmarked values to evaluate other applied models. In addition, seven other empirical models (by a various number of input variables) were chosen and applied in this study. These empirical models are Penman (most meteorological factors), Hargreaves-Samani (temperature-based), Priestley- Taylor (radiation-based), Blaney Criddle (temperature based), Makkink (temperature and radiation), Ouddin (temperature based) and Pan evaporation. Table 2 lists the mathematical formulae for these models in their original versions. Overall, the values of Kpan, ranging from a maximum value of around 0.835, a minimum value of 0.570 and a corresponding mean equal to 0.717.

Table 2. Empirical models used in this study for estimating ET_0

Empirical Models	**Equations**
FAO-56 PM (Allen et al. 2000)	$ET_0 = \frac{0.408(R_n - G) + 900\gamma \frac{U_2}{T_{mean}+273}(e_s - e_a)}{\Delta + \gamma(1 + 0.34U_2)}$
Penman (1948)	$ET_0 = \frac{\Delta.R_n + \gamma.(2.625 + 0.000479u2)(es - ea)}{\Delta + \gamma}$
Hargreaves–Samani (1985)	$ET_0 = 0.0023\ (Tmax - Tmin)^{0.5}(T + 17.8)\ Ra$
Priestley–Taylor (1972)	$ET_0 = 1.26\frac{\Delta}{\Delta + \gamma}(R_n - G)$
Blaney-Criddle (Blaney 1952)	$ET_0 = a + b[p(0.46T + 8.13)]$
Makkink (1957)	$ET_0 = C_{Mak}\frac{1}{\lambda}\frac{\Delta}{\Delta + \gamma}R_s$
Ouddin (Oudin et al. 2005)	$ET_0 = R_s[(T + 5)/100)]$

Pan evaporation (Trajkovic &Kolakovic 2010)	$ET_0 = K_p\ E_{pan}$

Where, ET_0 is the daily reference evapotranspiration (mm d−1), Rn ($MJ.m^{-2}.d^{-1}$) refers to the net radiation, G ($MJ.m^{-2}.d^{-1}$) indicates soil heat, γ (kPa $^oC^{-1}$) is the psychometric constant, U_2 (m s^{-1}) is the average daily wind speed at 2 m height, T (^oC) refers to the average daily air temperature, es and ea refer to the saturation and actual vapor pressures (kPa), respectively, es-ea indicates the saturation vapor pressure deficit (kPa), and Δ (kPa $°C^{-1}$) indicates the slope of the saturation vapor pressure curve, Ra ($MJ.m^{-2}.d^{-1}$) indicates extraterrestrial radiation, C_{MAK} is an empirical coefficient depending on climate conditions, p is the mean daily percentage of annual daytime hours, kp is the pan coefficient, Epan (mm day^{-1}) refers to the pan evaporation.

2.4. **Extreme Gradient Boosting (XGB) model**

The XGB (Chen et al. 2016) is a popular ML algorithm that is widely used for supervised learning tasks such as classification and regression. It belongs to the family of gradient boosting algorithms, which combine multiple weak models (such as decision trees) to form a strong model that can make accurate predictions on new data (Murorunkwere et al. 2023). XGB is known for its speed, scalability, and accuracy, and it has won multiple Kaggle competitions and other ML challenges. One of the key features of XGB is its ability to handle missing data and outliers effectively. XGB uses a technique called regularization, which penalizes complex models to prevent overfitting and improve generalization performance (Bhati et al. 2021, Chelgani et al. 2023). It also uses a technique called gradient boosting, which iteratively adds new weak models to the ensemble, with each new model correcting the errors of the previous models. This approach allows XGB to achieve high accuracy while avoiding the common pitfalls of

overfitting and bias. In addition to its performance and accuracy, XGB also offers a number of useful features for ML practitioners, such as early stopping, cross-validation, and feature importance analysis. These features make it easy to optimize hyperparameters, prevent overfitting, and interpret the results of the model. XGB can be categorized as a capable algorithm which is suitable for handling ML tasks (Begam et al. 2023).

2.5. Particle Swarm Optimization (PSO)

Proposed by Kennedy and Eberhart in 1995, PSO is a population-based stochastic optimization technique inspired by the collective behavior of flocking birds. In this method, each candidate solution is represented as a particle, and a collection of these particles forms a swarm. Every particle possesses a position and a velocity, which are updated during the k-th iteration using Equations (1) and (2).

$$\boldsymbol{v}_i^{k+1} = w\boldsymbol{v}_i^k + c_1\boldsymbol{r}_1\left(\boldsymbol{p}_i^k - \boldsymbol{x}_i^k\right) + c_2\boldsymbol{r}_2\left(\boldsymbol{p}_{gbest}^k - \boldsymbol{x}_i^k\right) \quad (1)$$

$$\boldsymbol{x}_i^{k+1} = \boldsymbol{x}_i^k + \boldsymbol{v}_i^{k+1} \quad (2)$$

where $\boldsymbol{x}_i^k$ and $\boldsymbol{v}_i^k$ represent the position and velocity of the ith particle at the kth iteration, respectively. $\boldsymbol{p}_i^k$ and $\boldsymbol{p}_{gbest}^k$ denote the personal best position of the ith particle and the global best position of the swarm, respectively. w is the inertia weight. c_1 and c_2 are cognitive and social acceleration coefficients determining the relative importance of $\boldsymbol{p}_i^k$ and $\boldsymbol{p}_{gbest}^k$. $\boldsymbol{r}_1$ and $\boldsymbol{r}_2$ are uniformly distributed random vectors within the interval [0, 1] (Nasiri et al., 2022).

2.6. Marine Predators Algorithm (MPA)

The MPA (Faramarzi et al. 2020) is a recent optimization algorithm inspired by the hunting behavior of marine predators, such as sharks and dolphins. The MPA algorithm works by simulating the movement of a group of predators in search of a prey target. Each predator in the group represents a candidate solution to the optimization problem, and their movements are guided by a set of rules that mimic the behavior of marine predators.

The MPA algorithm has been shown to be effective in solving a wide range of optimization problems, including continuous and discrete optimization problems, as well as multi-objective optimization problems. One of the key advantages of the MPA algorithm is its ability to balance exploration and exploitation of the search space (Sun et al. 2023). The algorithm is designed to explore the search space broadly in the early stages of the search, and then focus on exploiting promising regions as the search progresses. This helps to avoid getting trapped in local optima and improves the chances of finding the global optimum (Ewees et al. 2022). In terms of mathematical equation, when current iteration is in the first third of a maximum number of iterations (i.e., first stage of MPA), the best strategy for predator is not moving at all (Faramarzi et al. 2020). Note that this strategy leads to exploration. The mathematical formulation of this strategy is as follows:

$$\vec{\eta}_i = \vec{R}_B \otimes \left(\overrightarrow{Elite_i} - \vec{R}_B \otimes \overrightarrow{Prey_i}\right) \quad i = 1, \ldots, n \tag{3}$$

$$\overrightarrow{Prey_i} = \overrightarrow{Prey_i} + 0.5 \times \vec{R} \otimes \vec{\eta}_i \tag{4}$$

where $\vec{\eta}_i$ denotes the step size, $\vec{R}_B$ represents the random vector generated by Brownian motion, $\overrightarrow{Elite_i}$ is the matrix built by the top predator with the best fitness, n denotes the population size, and $\vec{R}$ is a random vector, uniformly distributed in [0,1] (Liang et al. 2022).

During the transition from exploration to exploitation stage (i.e., second stage of MPA), the population is divided into two groups: one for global exploration, where the predator explores the search space using Brownian motion, and the other for local exploitation, where the prey is exploited using Lévy motion. Finally, during the exploitation stage (i.e., third stage of MPA), which occurs in the last two-thirds of the maximum allowed iterations when the predator is slower than the prey, the predator uses the Lévy migration strategy (Ewees et al. 2022, Liang et al. 2022). MEALPY open-source library (Van Thieu and Mirjalili, 2023) was used for implementing the MPA algorithm.

2.7. **Combination of meteorological variables for ET_0 estimation**

This study aims to compare the performances of several empirical models and a ML and nature-inspired optimization technique to predict ET_0. Tmean, Tmax, Tmin, SSH, W, RHmean, RHmax, Rhmin, extraterrestrial solar radiation (Ra), and Epan values are presented as inputs to XGB and XGB-MPA models for constructing ET_0 prediction models. Twenty independent runs were performed for XGB and XGB-MPA models in each scenario to ensure the robustness of the results and evaluate the performance of models more accurately. Various input combinations of the XGB and XGB-MPA models constructed for estimating ET_0 values are presented in Table 3. Also, Figure 2 shows the flowchart of the current study.

Table 3. Various input combinations of the established models

No.	Input(s)	Output	Models	
1	Tmean	ET_0	XGB1	XGB-MPA1

2	Tmean, Tmax, Tmin	ET_0	XGB2	XGB-MPA2
3	Tmean, Tmax, Tmin, SSH	ET_0	XGB3	XGB-MPA3
4	Tmean, Tmax, Tmin, SSH, W	ET_0	XGB4	XGB-MPA4
5	Tmean, Tmax, Tmin, SSH, W, RHmean	ET_0	XGB5	XGB-MPA5
6	Tmean, Tmax, Tmin, SSH, W, Rhmean, Rhmax, Rhmin	ET_0	XGB6	XGB-MPA6
7	Tmean, Tmax, Tmin, SSH, W, Rhmean, Rhmax, Rhmin, Ra	ET_0	XGB7	XGB-MPA7
8	Tmean, Tmax, Tmin, SSH, W, Rhmean, Rhmax, Rhmin, Ra, Epan	ET_0	XGB8	XGB-MPA8

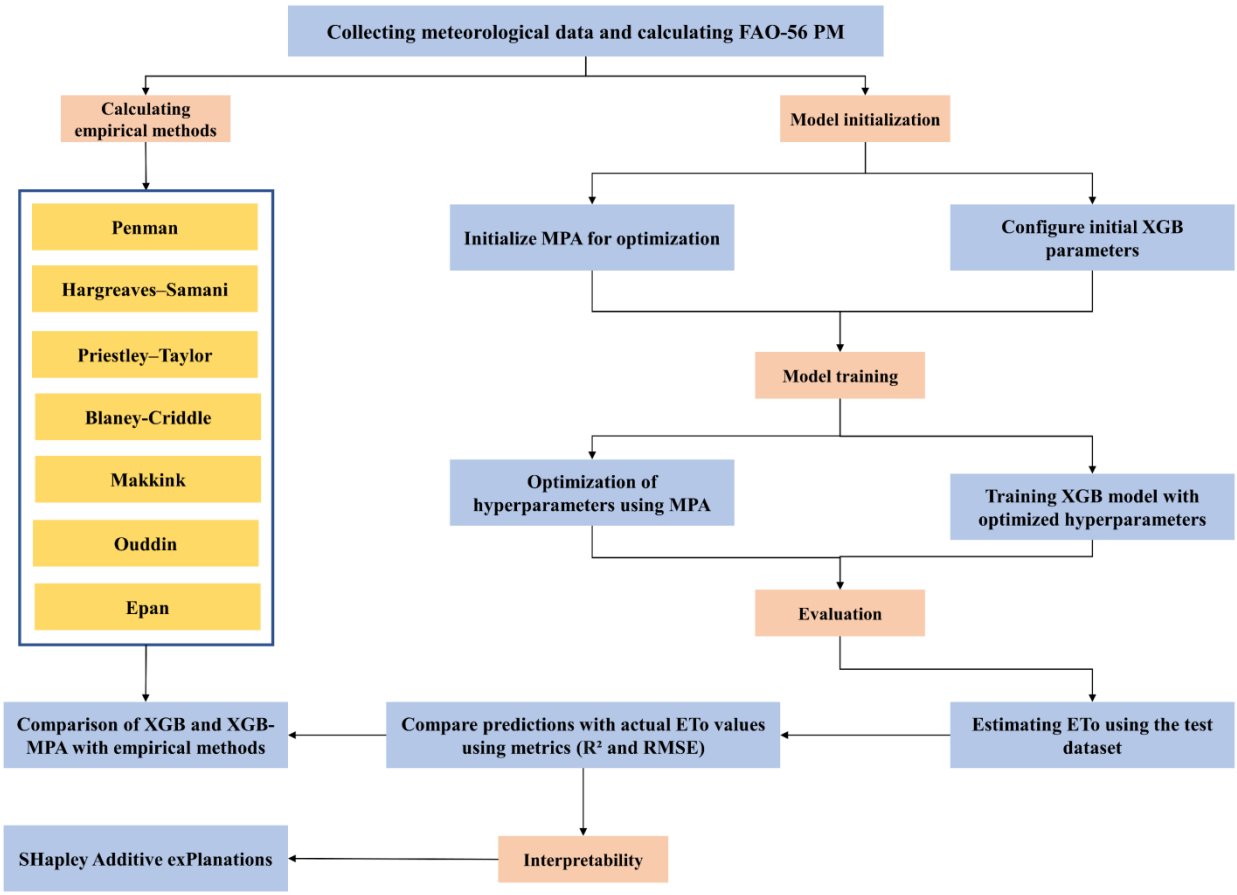

Figure 2. Flowchart of the current study

2.8. SHAP post-processing method

SHAP (short for SHapley Additive exPlanations) (Lundberg &Lee 2017) is a recently developed algorithm that provides a framework for interpreting the predictions of complex ML models. It is based on the Shapley value from cooperative game theory, which is a mathematical concept used to distribute the payout of a game among its players in a fair way. In the context of ML, SHAP uses the Shapley value to assign a contribution score to each feature in a prediction, indicating how much each feature contributes to the prediction compared to the other (Heuillet et al. 2022) features .

One of the key advantages of SHAP is its ability to provide both local and global explanations of a model's predictions. Local explanations show how a model arrived at a particular prediction for a specific instance, while global explanations show how the model behaves in general and which features are most important overall. This is particularly useful in situations where the performance of the model needs to be justified or its behavior needs to be understood. Another strength of the SHAP algorithm is its versatility and compatibility with a wide range of ML models and architectures. It can be used with both linear and non-linear models, as well as with tree-based models, deep learning models, and ensemble models (Fatahi et al. 2022, Zhang et al. 2023). This makes it a powerful tool for interpreting the predictions of complex models in a variety of domains, from healthcare and finance to natural language processing and computer vision. SHAP presents a remarkable understanding in the realm of explainable AI as it provides a robust and versatile approach to discerning the outcomes of intricate ML models.

2.9. **Evaluation metrics**

To evaluate the performance of the proposed models, statistical measures such as the coefficient of determination (R^2) and root mean square error (RMSE) were utilized. The R^2 value indicates the linear correlation between the predicted and observed values, while the RMSE represents the overall accuracy of the simulation. R^2 is dimensionless and can be range from 0 to 1; unit of RMSE is mm/day in this study and it can be ranged from 0 to ∞. These statistical measures are presented as follows:

$$R^2=\left(\frac{\sum_{i=1}^{n}(ET_i^o-\overline{ET^o})(ET_i^p-\overline{ET^p})}{\sqrt{\sum_{i=1}^{n}(ET_i^o-\overline{ET^o})^2\sum_{i=1}^{n}(ET_i^p-\overline{ET^p})^2}}\right)^2 \quad (5)$$

$$RMSE=\sqrt{\frac{1}{n}\sum_{i=1}^{n}(ET_i^p-ET_i^o)^2} \quad (6)$$

where, n denotes the number of the data; ET_i^o and ET_i^p are the i^{th} observed and forecasted ET_0, respectively; $\overline{ET^o}$and $\overline{ET^p}$ are the average of the observed and forecasted ET_0, respectively.

3. Results

The proposed model was implanted using Python programming language and Scikit-learn ML library (Pedregosa et al., 2011). The experiments were run on an Intel Core i7-6700HQ, 2.60GHz CPU with 12 GB RAM, running Windows 10 operating system. In all experiments, the XGB parameters for the XGB-MPA model were tuned by the MPA algorithm, and the parameters for the XGB model were acquired by trial and error. The obtained parameters for the best models (i.e., XGB-MPA7 and XGB7) are shown in Table 4. Moreover, for the MPA

algorithm, the default values of the parameters were used except for two parameters: the population size was set to 50, and the maximum number of train epochs was set to 10.

Table 4. Parameter setting for machine learning models (for the best XGB-based scenario (XGB7) and the best XGB-MPA-based scenario (XGB-MPA7))

Parameter	Value
XGB7	
Base learner	Gradient boosted tree
Number of gradient boosted trees	100
Learning rate	0.3
Lagrange multiplier	0
Maximum depth of trees	6
XGB-MPA7	
Base learner	Gradient boosted tree
Number of gradient boosted trees	300
Learning rate	0.060
Lagrange multiplier	0.007
Maximum depth of trees	6

The results of ET_0 estimation in testing set with various data input combinations of XGB model are shown in Table 5. The XGB model has been tested using seven different variations (XGB1-XGB8), and for each variation, the model has been tested using 20 different random state values (0-19). Looking at the table, we can see that the model's performance varies depending on the random state value used during training. According to the average statistical metrics, the lowest RMSE (0.2727 mm/day) and highest R^2 (0.9889) values were produced with the 7th combination (inputs: Tmean, Tmax, Tmin, SSH, W, Rhmean, Rhmax, Rhmin, and Ra). Moreover, the precision of ET_0 prediction generally enhanced during the testing phase with an increase in the number of meteorological input variables utilized in the models. For example, analyzing the

367 average values, XGB1 attained an R^2 score of 0.7603and an RMSE of 1.2675(mm/day), whereas
368 XGB8 obtained an R^2 score of 0.9881and an RMSE of 0.2831 (mm/day). These findings suggest
369 that XGB8 outperformed XGB1. Similarly, we can ascertain the model that shows the best
370 overall performance by comparing the metrics across various random states. In addition, when
371 the R^2 and RMSE values of the meteorological variables of model 2, 3, 4 and 5 combinations are
372 examined, it is found that the prediction performance of the XGB model increases significantly
373 especially from combination 2 to 3, 3 to 4 and 4 to 5. Consequently, one can deduce that the
374 influence of supplementary meteorological factors such as SSH, W, and RHmean on the ET_0
375 prediction is significant. In conclusion, the incorporation of the W variable in the model has a
376 noteworthy impact on the ET_0 prediction, specifically regarding the transportation of water vapor
377 from the crop surface. The SSH variable considers the availability of solar energy, and the Epan
378 variable accounts for water evaporation from an open pan placed under specific meteorological
379 conditions.

380 **Table 5.** Results for the XGB model during the test section (the best R^2 and RMSE values for
381 each run are in bold)

	XGB1		XGB2		XGB3		XGB4		XGB5		XGB6		XGB7		XGB8	
Random State	R^2	RMSE	R^2	RMSE	R^2	RMSE	R^2	RMSE	R^2	RMSE	R^2	RMSE	R^2	RMSE	R^2	RMSE
0	0.7622	1.2611	0.7447	1.3194	0.8324	1.071	0.9348	0.6839	0.9543	0.5514	0.9542	0.5518	0.9889	0.2729	0.9865	0.3033
1	0.7602	1.2678	0.743	1.3268	0.823	1.099	**0.9386**	**0.6594**	0.9562	0.5398	0.9543	0.5507	0.989	0.2721	0.9874	0.2917
2	0.7644	1.2563	0.7486	1.311	0.83	1.075	0.9365	0.6792	0.9566	0.537	0.9536	0.5554	0.99	0.2598	**0.9896**	**0.2648**
3	0.763	1.2603	0.7527	1.2949	0.8306	1.0701	0.9365	0.6748	0.9558	0.5418	0.9561	0.5401	0.9884	0.2803	0.9879	0.2843
4	0.7619	1.2633	0.7497	1.3046	0.8263	1.0873	0.9378	0.6668	0.9579	0.5288	**0.9579**	**0.53**	0.9891	0.2706	0.9885	0.2779
5	0.7564	1.2784	0.7498	1.3104	0.8301	1.0775	0.9357	0.6791	0.9559	0.5421	0.9541	0.5521	**0.9903**	**0.2547**	0.9883	0.2792
6	0.7607	1.2663	0.7488	1.3115	0.8286	1.082	0.9359	0.6733	0.9561	0.5402	0.9553	0.5449	0.9885	0.281	0.9869	0.299
7	0.7579	1.2749	0.7433	1.324	0.8252	1.0883	0.9337	0.6856	**0.959**	**0.5228**	0.9539	0.5536	0.9882	0.2816	0.9882	0.2828
8	0.7634	1.2579	0.7499	1.3049	0.8332	1.0648	0.9364	0.6818	0.9546	0.5499	0.9558	0.5431	0.9897	0.2626	0.9895	0.2647
9	0.7567	1.277	0.7462	1.3159	0.8294	1.0766	0.9335	0.6859	0.9565	0.5381	0.9518	0.5668	0.9884	0.2799	0.988	0.283
10	0.7584	1.2731	0.7522	1.2989	0.8259	1.0959	0.9368	0.6713	0.9559	0.5416	0.9543	0.5519	0.9889	0.2761	0.988	0.2842
11	0.7554	1.2803	0.7542	**1.2944**	0.8323	1.0643	0.9347	0.6828	0.9552	0.5466	0.9555	0.5438	0.9898	0.2611	0.9887	0.2749
12	0.7587	1.2707	0.7449	1.3212	**0.8343**	**1.0594**	0.933	0.6896	0.9542	0.5515	0.9529	0.5599	0.9883	0.2809	0.9879	0.286
13	0.7599	1.2694	0.7487	1.3087	0.8297	1.0733	0.9377	0.6667	0.9582	0.5275	0.9568	0.5357	0.9881	0.2813	0.986	0.3067

14	0.7615	1.2632	0.7474	1.3146	0.8324	1.0704	0.9349	0.6764	0.9557	0.5424	0.9534	0.5563	0.9884	0.2771	0.9883	0.28
15	0.7611	1.2649	0.7433	1.3255	0.8256	1.089	0.938	0.6646	0.9567	0.5372	0.9521	0.5649	0.9886	0.2783	0.9886	0.2788
16	0.7588	1.2736	**0.7546**	1.2973	0.8242	1.1002	0.9368	0.6753	0.9555	0.5444	0.9559	0.542	0.9897	0.262	0.9879	0.2856
17	**0.7646**	**1.2554**	0.7469	1.3145	0.8295	1.078	0.9339	0.6865	0.9565	0.5384	0.9564	0.5385	0.9887	0.2759	0.9886	0.2771
18	0.7604	1.2682	0.7445	1.3225	0.8295	1.0786	0.9369	0.6762	0.9556	0.5435	0.9541	0.5519	0.9882	0.2814	0.9887	0.2758
19	0.7605	1.267	0.7458	1.3196	0.8186	1.111	0.9357	0.6801	0.9551	0.547	0.9523	0.5629	0.9897	0.2646	0.9882	0.2816
Average	0.7603	1.2675	0.748	1.312	0.8286	1.0806	0.9359	0.677	0.9561	0.5406	0.9545	0.5498	0.9889	0.2727	0.9881	0.2831

Test estimation results of the XGB-MPA model are presented in Table 6. When evaluated according to the average of the test statistics, it was revealed that the combination number 7 produced the most accurate predictions with the highest R^2 (0.9958) and lowest RMSE (0.1713 mm/day) values. In addition, it is noteworthy that the increase in the number of meteorological input variables used in the models increases the success of ET_0 prediction. Because all meteorological variables used are directly dependent on ET_0 parameters. In addition, it was revealed that the accuracy of estimating the MPA-optimized XGB algorithm during the test phase was slightly improved according to increasing R^2 and decreasing RMSE values. Examining the average values of the table, XGB-MPA1 obtained an R^2 value of 0.7864 and an RMSE of 1.1931 (mm/day), whereas XGB-MPA2 achieved an R^2 score of 0.8054 and an RMSE of 1.1384 (mm/day). These findings indicate that XGB-MPA2 exhibited superior performance compared to XGB-MPA1. According to the results of 20 different random states, the XGB-MPA2 algorithm consisting of Tmean, Tmax, Tmin meteorological input combinations has an R^2 score of 0.8054 and RMSE of 1.1384 mm/day, while the XGB-MPA5 algorithm consisting of Tmean, Tmax, Tmin, SSH, W, RHmean input combinations has an R^2 score of 0.9682 and RMSE of 0.4598 mm/day. Accordingly, it can be inferred that the SSH, W, RHmean variables added to the model contribute significantly to the ET_0 prediction. Moreover, it is noteworthy that the most accurate prediction results are obtained when all meteorological variables are presented as inputs to the XGB-MPA7 model.

Table 6. Results for the XGB-MPA model during the test section (the best R^2 and RMSE values for each run are in bold)

Random State	XGB-MPA1		XGB-MPA2		XGB-MPA3		XGB-MPA4		XGB-MPA5		XGB-MPA6		XGB-MPA7		XGB-MPA8	
	R^2	RMSE	R^2	RMSE	R^2	RMSE	R^2	RMSE	R^2	RMSE	R^2	RMSE	R^2	RMSE	R^2	RMSE
0	0.7852	1.1962	0.8051	1.1397	0.8676	0.9386	0.9496	0.5813	0.9686	0.4571	0.969	0.455	0.9956	0.1752	**0.9959**	0.1695
1	0.7852	1.1951	0.804	1.1424	0.8681	0.9374	0.9485	0.5862	0.968	0.4612	0.9689	0.4549	0.9955	0.1776	0.9953	0.1798
2	0.787	1.1915	0.8057	1.1369	0.8686	0.935	0.9494	0.5821	0.9681	0.4608	0.9687	0.4567	**0.9961**	**0.1649**	**0.9959**	**0.1681**
3	0.7864	1.1936	0.8056	1.1379	0.868	0.9373	0.9502	**0.5777**	**0.9687**	**0.4559**	**0.9696**	**0.45**	0.9959	0.1687	**0.9959**	0.1694
4	0.7867	1.1925	0.8049	1.1399	0.8683	0.9365	0.9497	0.5804	0.9677	0.4635	0.9694	0.4515	0.9957	0.1713	0.9958	0.1702
5	0.7856	1.1953	0.8066	**1.1335**	**0.8696**	**0.932**	0.9497	0.58	0.9681	0.4604	0.9688	0.456	0.9957	0.1718	0.9957	0.1736
6	0.7876	1.1892	0.8064	1.1352	0.8687	0.9348	**0.9504**	0.5785	0.9681	0.4607	0.9682	0.46	0.9958	0.1714	0.9956	0.1762
7	0.7857	1.1951	0.8052	1.1388	0.8678	0.9375	0.9493	0.5826	0.9682	0.4594	0.9684	0.4584	0.9958	0.1705	0.9955	0.1758
8	0.7868	1.1927	0.8051	1.139	0.8684	0.9363	0.9493	0.5826	0.9683	0.4588	0.9691	0.4534	0.9957	0.1712	0.9957	0.1728
9	0.787	1.1918	0.8053	1.1387	0.8693	0.9337	0.9491	0.5839	0.9682	0.4598	0.9692	0.453	0.9957	0.1712	0.9955	0.1776
10	0.7871	1.1901	0.8045	1.1413	0.8684	0.9365	0.9496	0.5804	0.9686	0.4566	0.9689	0.4554	0.9957	0.1722	0.9956	0.1728
11	0.7866	1.1927	0.8056	1.138	0.8684	0.9357	0.9492	0.5839	0.9678	0.4628	0.969	0.4547	0.9958	0.1707	0.9956	0.1762
12	0.7859	1.1951	0.8045	1.1408	0.8675	0.9384	0.9494	0.5822	0.9682	0.4594	0.969	0.4543	0.9957	0.1722	0.9956	0.1741
13	0.7862	1.1932	0.8061	1.1367	0.8693	0.9329	0.9495	0.5823	0.968	0.4613	0.9686	0.4569	0.9955	0.1753	0.9954	0.1803
14	0.7863	1.1942	0.8044	1.1416	0.8675	0.9384	0.95	0.5806	0.9682	0.4599	0.9685	0.458	0.9958	0.1705	**0.9959**	0.169
15	0.7858	1.1945	0.8062	1.1358	0.8684	0.9357	0.9498	0.5799	0.9682	0.4593	0.969	0.4541	0.9957	0.1721	0.9958	0.1717
16	**0.7878**	**1.1889**	**0.8071**	1.1338	0.8684	0.9362	0.9494	0.5823	0.9684	0.4582	0.9692	0.4532	0.996	0.1664	0.9955	0.1765
17	0.7867	1.1922	0.8044	1.1405	0.8665	0.9423	0.95	0.5796	0.9685	0.4572	0.9689	0.4556	0.9958	0.1709	0.9958	0.1717
18	0.7864	1.193	0.8048	1.1403	0.8671	0.9401	0.9498	0.5813	0.9682	0.4602	0.9692	0.4531	0.9958	0.171	0.9958	0.1724
19	0.7858	1.1953	0.8059	1.1367	0.8679	0.9375	0.9496	0.5814	0.9675	0.4644	0.9683	0.4596	0.9958	0.1701	0.9958	0.1705
Average	0.7864	1.1931	0.8054	1.1384	0.8682	0.9367	0.9496	0.5815	0.9682	0.4598	0.9689	0.4552	0.9958	0.1713	0.9957	0.1734

In Figure 3, the FAO-56-based ET_0 values and the ET_0 values estimated by various empirical equations were evaluated employing a scatter plot. Furthermore, the relationship between the benchmarked and predicted values in the scattering diagrams was evaluated. Accordingly, the optimal model was chosen as the empirical equation showing distribution on the regression line. According to these criteria, it was found that Ouddin (2005) equation had the highest similarity with FAO-56-based ET_0. In addition, it can be seen that the Epan values have the weakest relationship with the ET_0 values because they show random scattering. In addition, it is noteworthy that the ET_0 values calculated with the (Hargreaves &Samani 1985) and (Penman 1948) equations deviate significantly from the FAO-56-based ET_0 values, especially at values greater

than 5 mm/day, and the errors increase. The ET_0 values calculated according to the (Oudin et al. 2005), (Makkink 1957) and (Priestley &Taylor 1972) equation were found to deviate significantly from the FAO-56-based ET_0 values, especially at values greater than 10 mm/day.

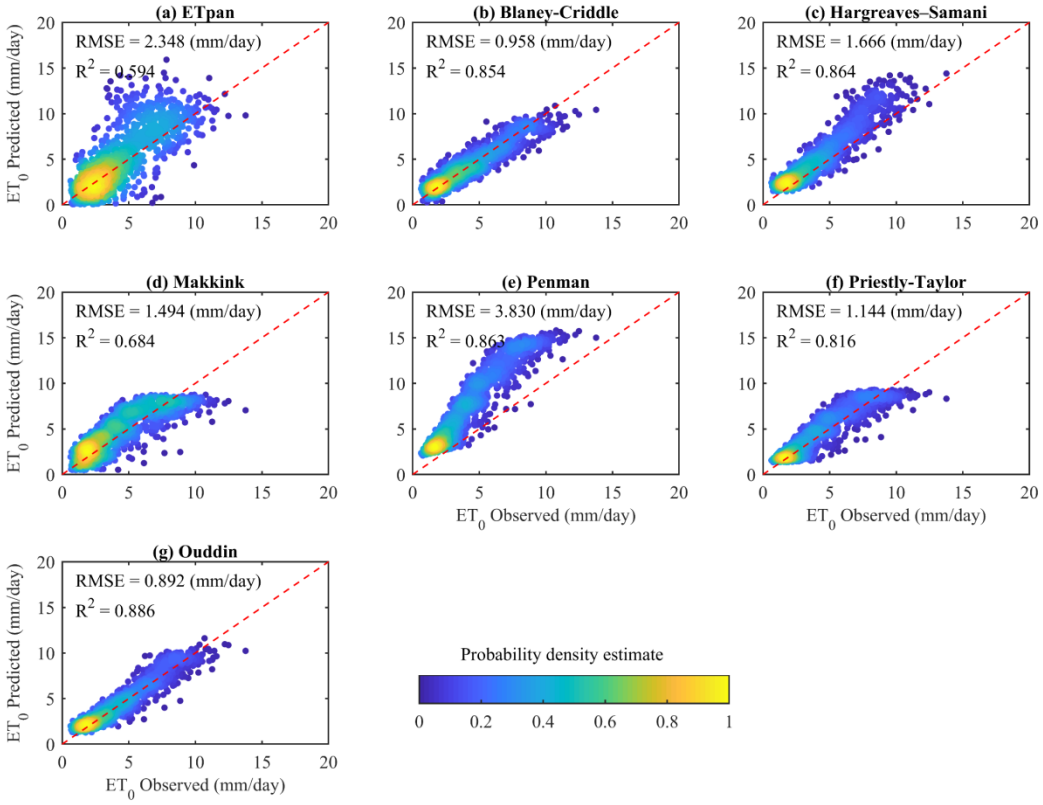

Figure 3. Comparison of empirical models through test section scatter plots

In Figure 4, the estimation results of the XGB model established with the combinations of various meteorological variables for the estimation of ET_0 values are shown. In the scatter diagrams, the relationship between the benchmarked and predicted values was interpreted according to the closeness to the regression line. Accordingly, the XGB7 model, which is distributed over the regression line, was chosen as the optimal model. It is also noteworthy that the XGB 2 model has the lowest accuracy. In addition, according to the scattering diagrams, it is

seen that there is a little deviation from the regression line in the estimation results of the XGB1, 2 and 3 models above 10 mm/day. In addition, in other estimation models, it is seen that it gathers around the regression line. When evaluating all scatter plots, it is observed that the combination of XGB4-7 models significantly improves the ET_0 prediction performance compared to the XGB1-3 combinations. Therefore, it can be inferred that presenting wind speed values as input to the model significantly reduces the error value.

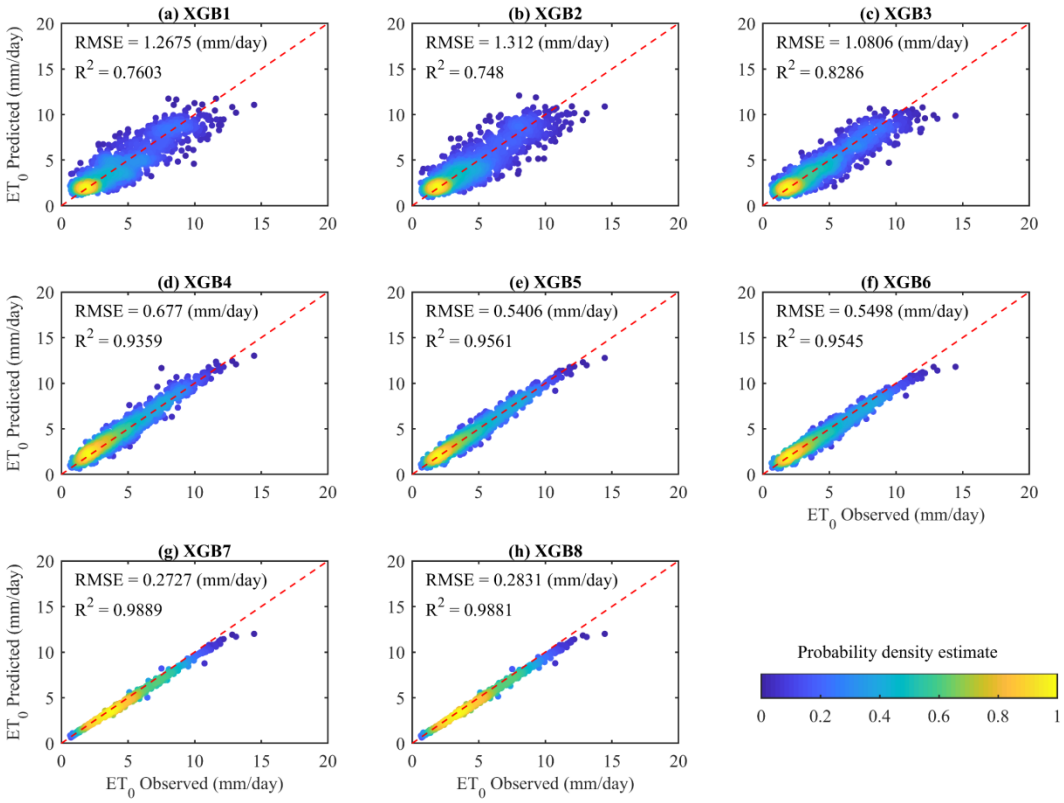

Figure 4. Evaluation of XGB model combinations used in ET_0 estimation through test section scatter plots

436 The prediction performance of tree-based XGB and bio-inspired MPA algorithms for ET_0
437 estimation is depicted in the scatter plots in Figure 5. Accordingly, the XGB7 model, distributed
438 over the regression line, was assessed as superior. It was revealed that the MPA algorithm
439 increased the prediction accuracy of the single XGB algorithm in estimating ET_0. In addition,
440 when the estimation results were evaluated according to the scattering diagrams, it was
441 determined that there was some deviation from the regression line in the estimation results of the
442 XGB-MPA1, 2 and 3 models above 10 mm/day values. It can be resulted that XGB-MPA4, 5, 6
443 and 7 estimation models have high accuracy due to their distribution around the regression line.
444 When the error values of the scatter diagrams were examined, it was seen that the error value
445 decreased to the hybrid model as of the XGB-MPA4 model. This can be explained by the
446 inclusion of wind speed values in the hybrid models.

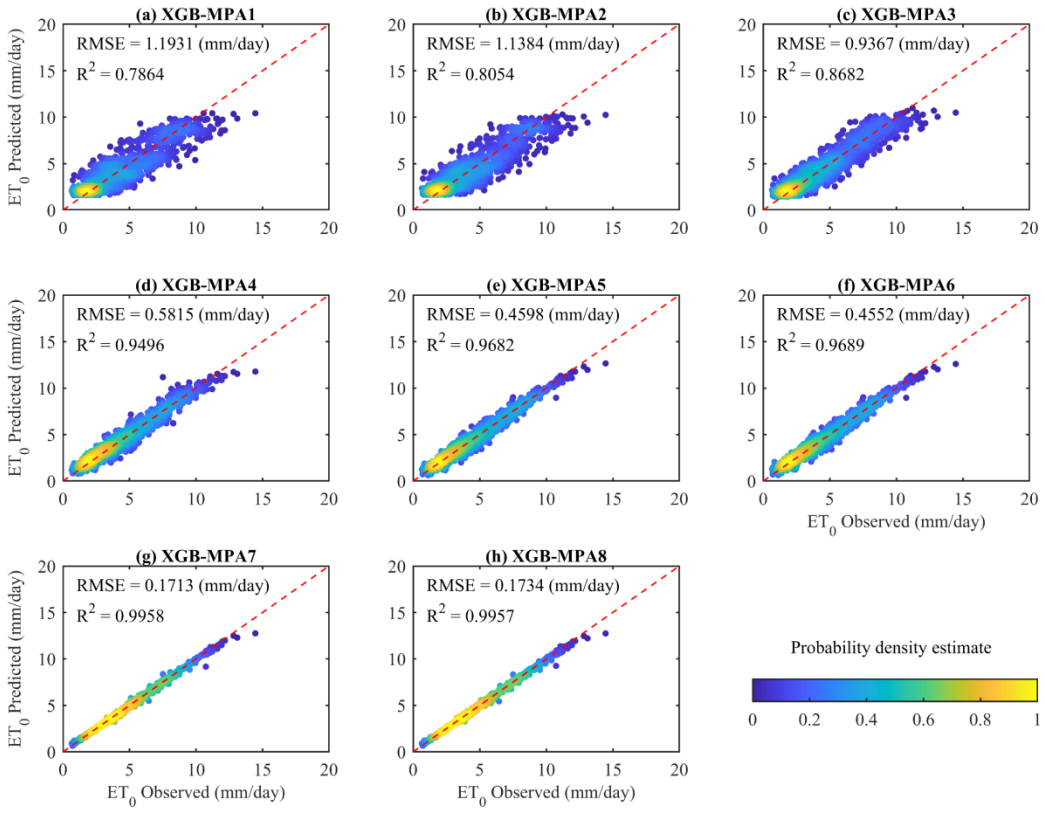

Figure 5. Evaluation of XGB-MPA model combinations used in ET_0 estimation through test section scatter plots

In Figure 6, the evaluation of the results of ET_0 estimation based on the FAO-56 method during the training and testing phases using empirical equations, XGB, and XGB-MPA algorithms are presented through boxplot graphs. The median, outliers, distribution, and percentile ranges of the ET_0 time series and estimated time series were determined to determine the most accurate model. According to the results, the Oudin et al. (2005) equation, XGB7, and XGB-MPA7 algorithms demonstrated the highest similarity and distribution in modeling ET_0 values during the training and testing phases. In addition, the Perman equation showed the weakest accuracy. Notably, all XGB and XGB-MPA models established had satisfactory prediction accuracy.

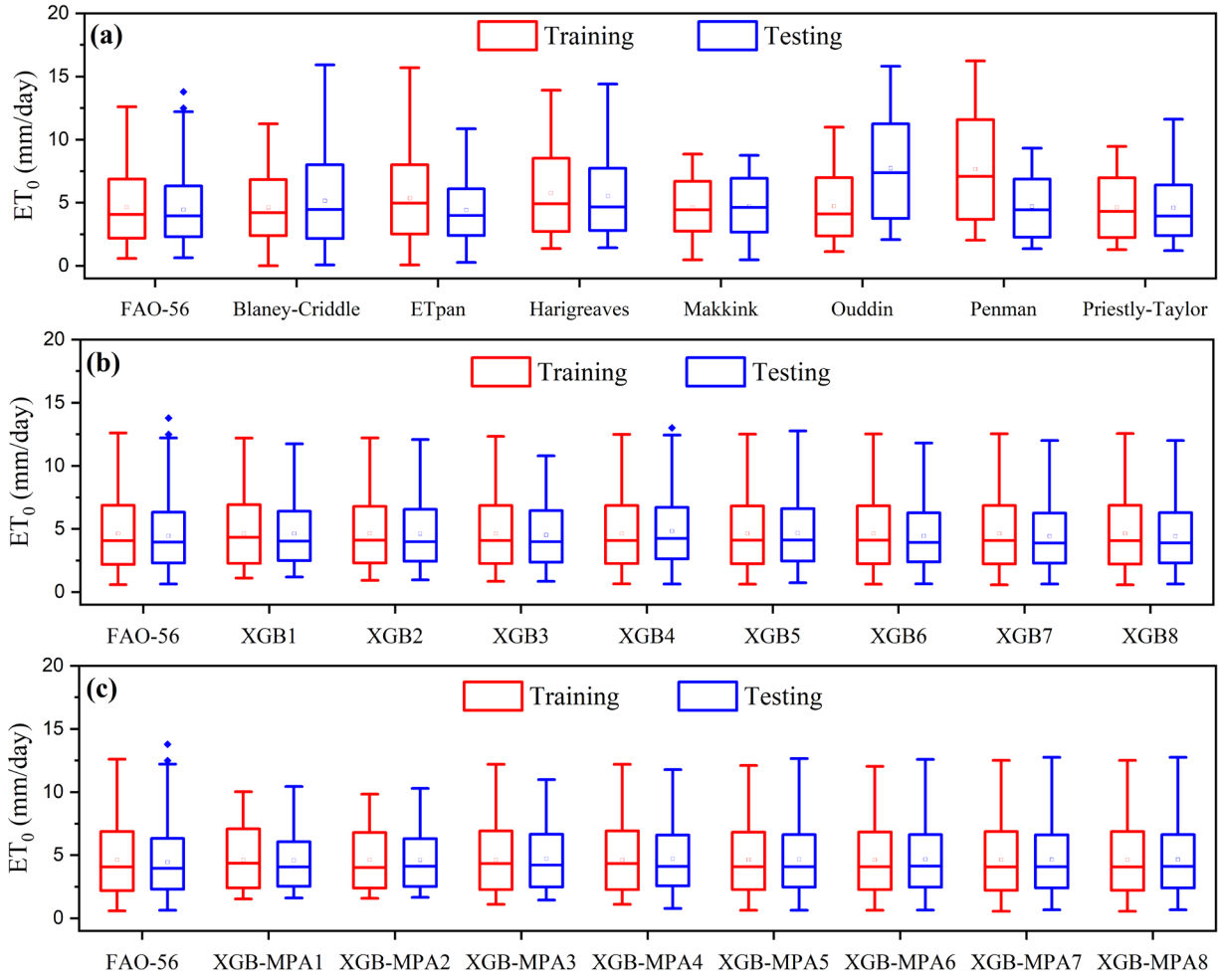

458

459 **Figure 6.** Box plots: (a) for empirical models, (b) for the XGB-based models, (c) for the XGB-

460 MPA-based models

461 The entire dataset was analyzed using SHAP to explore associations and identify variable

462 significance assessments to generate a robust ET_0 estimate. Figure 7 shows the SHAP beeswarm

463 plots of the variables used to estimate ET_0. Through these graphs, the direction and strength of

464 the effects of a particular sample on the model output can be evaluated. The x-axis location of

465 the point expresses the effect of the feature on the model output. The dots show the possible

466 positive effect on the right and the possible negative effect on the left. In Figure 8, the order of

467 importance from top to bottom showing the effect of the variables on the output is given. The
468 contribution of each feature to the model output is expressed through the length of the bar.
469 Accordingly, it has been determined that Tmax values have the highest importance in predicting
470 ET_0 values among all variables in the dataset, while RHmax values have the lowest importance.
471 In addition, it is seen that there is a positive relationship between estimated ET_0 values and
472 Tmax, Ra, W, SSH, Tmean, Epan, and Tmin values, and a negative relationship with RHmean,
473 RHmin and RHmax values.

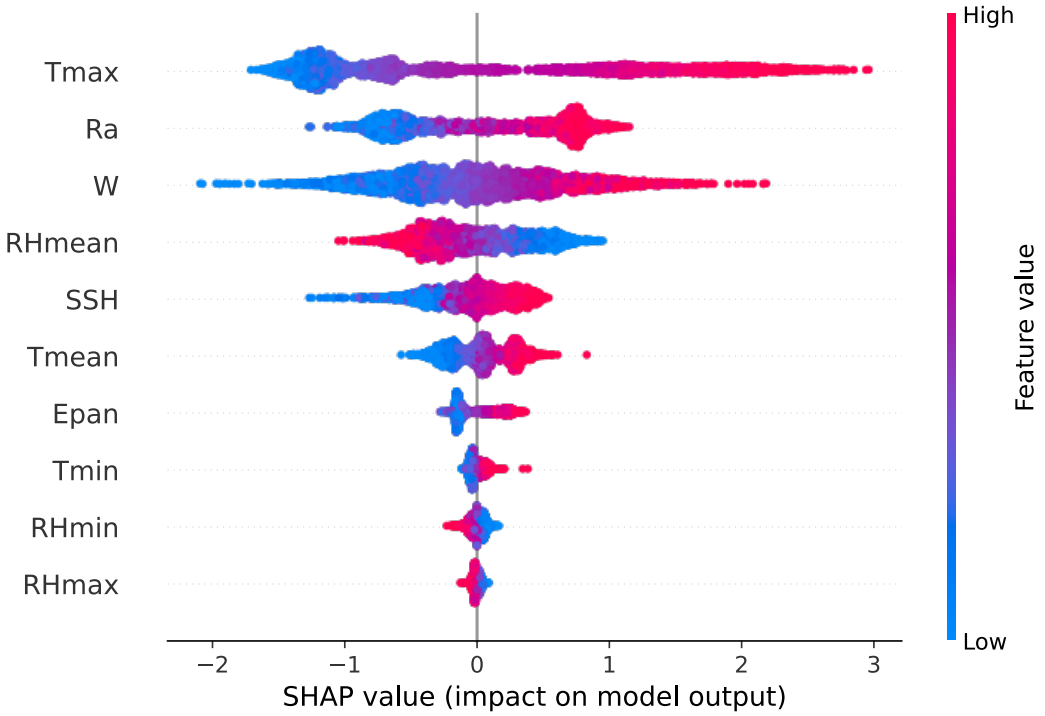

474

475 **Figure 7.** SHAP beeswarm plot

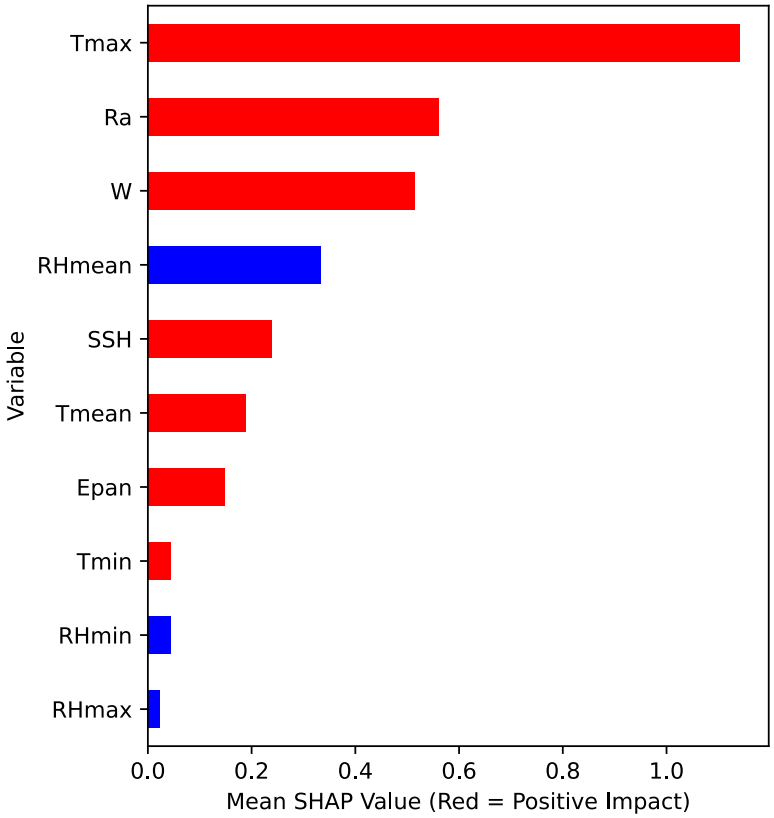

476

477 **Figure 8.** SHAP bar plot

478

479 Figure 9 compares the results of ET_0 estimation based on the FAO-56 method during the training
480 and testing phases using empirical equations and XGB-based models through Taylor diagrams.
481 The most accurate model was determined by comparing the correlation, RMSE, and standard
482 deviation values of the benchmarked and estimated time series on the Taylor diagram. According
483 to the results, the Oudin et al. (2005) equation, XGB7, and XGB-MPA7 algorithms provided the
484 most accurate results in predicting ET_0 values during the training and testing phases.

485

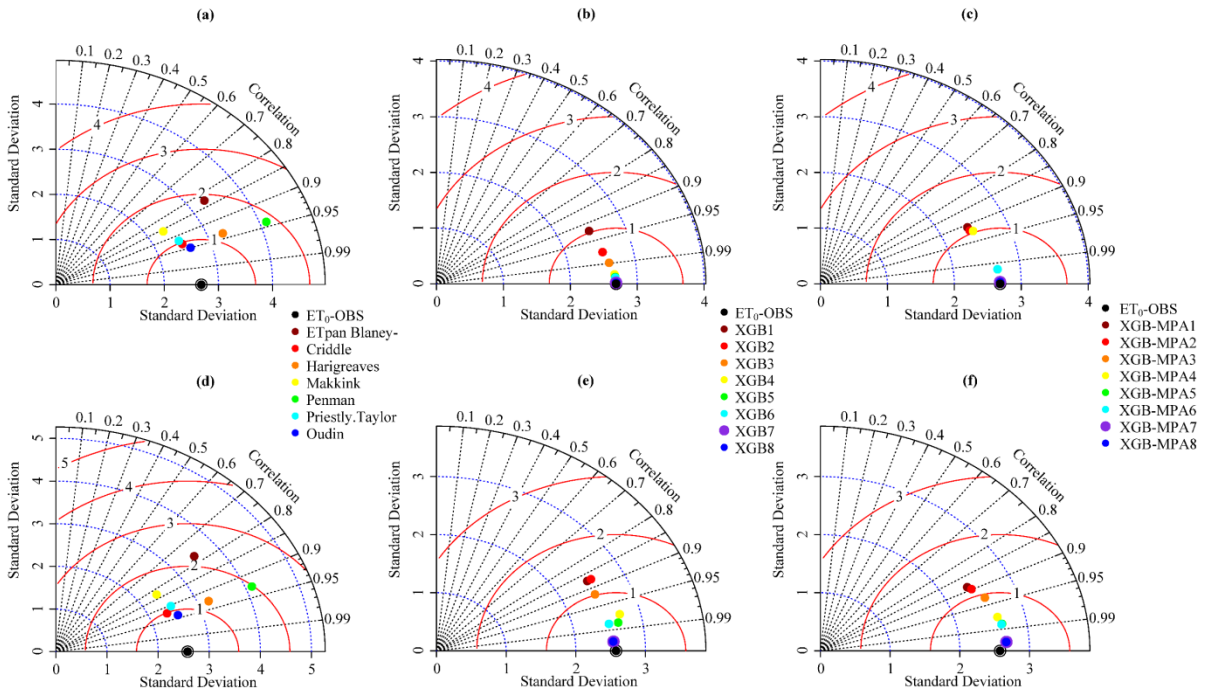

Figure 9. Taylor diagram of training set (a, b, and c) and testing set (d, e, and f)

Precise calculation of ET_0 is crucial in numerous areas, such as designing irrigation schedules, managing agricultural water, modeling crop growth, and evaluating drought conditions. This study aimed to compare the performance of several empirical models and ML and nature-inspired optimization techniques in predicting ET_0. FAO-56-based ET_0 values were selected as observed data and estimated with XGB and XGB-MPA. Tmean, Tmax, Tmin, SSH, W, RHmean, RHmax, Rhmin, and Epan values were presented as inputs to the XGB and XGB-MPA models for constructing the ET_0 prediction models. According to the presented findings, it can be concluded that wind speed, sunshine hours and average relative humidity are among the most important inputs of ET_0 simulator models in the study area, and the boundary values (minimum and maximum) of relative humidity and pan evaporation have not occupied a substantial role in estimation of this component.

Fan et al. (Fan et al. 2019) showed that ET_0 values could be predicted satisfactorily by using various ML algorithms with Tmax, Tmin, RH, wind speed at 2m height, extraterrestrial solar radiation (Ra) and global solar radiation (Rs) variables in China. Moreover, it has been determined that the LightGBM model outperforms other ML models with R^2 (1) and RMSE (0.08 mm/day) values in the testing phase. In this region, the estimation of daily ET_0 was primarily influenced by Tmax and W. At the same time, RH had a comparatively lesser impact and Tmin had the least influence. The average R^2 (0.9602) and RMSE (0.5064 mm/day) values in the testing phase of the GBM model showed satisfactory results in estimating ET_0. The study's results significantly overlap with Fan et al. (Fan et al. 2019) in terms of the performance of the GBM algorithm and the effect of the meteorological parameters used. However, the high effect of Tmin values in estimating ET_0 contradicts the study. In the study of Ferreira et al. (Ferreira &da Cunha 2020), ML and deep learning techniques were used to predict daily ET_0 values according to hourly temperature and relative humidity values. The study results showed that deep learning methods are superior in ET_0 prediction. It also supports the research on producing satisfactory outputs with the XGB algorithm. Yu et al. (Yu et al. 2020) proposed a new model named PSO-XGB using XGB and PSO of ET_0 values calculated according to the Penman-Monteith equation. As a result, it has been determined that the bio-inspired PSO algorithm improves the performance of the XGB model and the prediction accuracy increases with the increase in the number of meteorological input combinations. The XGB-MPA7 model with the most input variables gives the most accurate results in the study. The nature-inspired MPA algorithm overlaps with the study of Yu et al. (2020) in terms of increasing the success of the XGB model. Yan et al. (2021) estimated daily ET_0 using XGB and whale optimization algorithm (WOA) in arid and humid regions in China. The results showed that wind speed is the most

523 influential variable in the arid region, while the relative sunshine duration is more important in
524 the humid region. WOA-XGB models performed 40% higher than FAO-56 PM models. The
525 study results are consistent with the nature-inspired MPA improving the ET_0 prediction success
526 of XGB.

527 Histograms of the percentage changes of R^2 and RMSE values of ET_0 prediction models are
528 presented in Figure 10. The success of the prediction models was compared to the XGB1 and
529 XGB-MPA1 models. It was found that the model's performance was significantly improved by
530 increasing the number of input variables in ET_0 prediction. Accordingly, the XGB and XGB-
531 MPA models established with the input variables Tmean, Tmax, Tmin, SSH, W, RHmean,
532 RHmax, RHmin, and Epan emerged as superior models. In addition, the XGB7 model improved
533 the R^2 and RMSE values in the testing phase by 94.2% and 78.5%, respectively, in ET_0
534 prediction. Moreover, the XGB-MPA7 model improved the R^2 and RMSE values in the testing
535 phase by 95.9% and 85.6%, respectively, in ET_0 prediction.

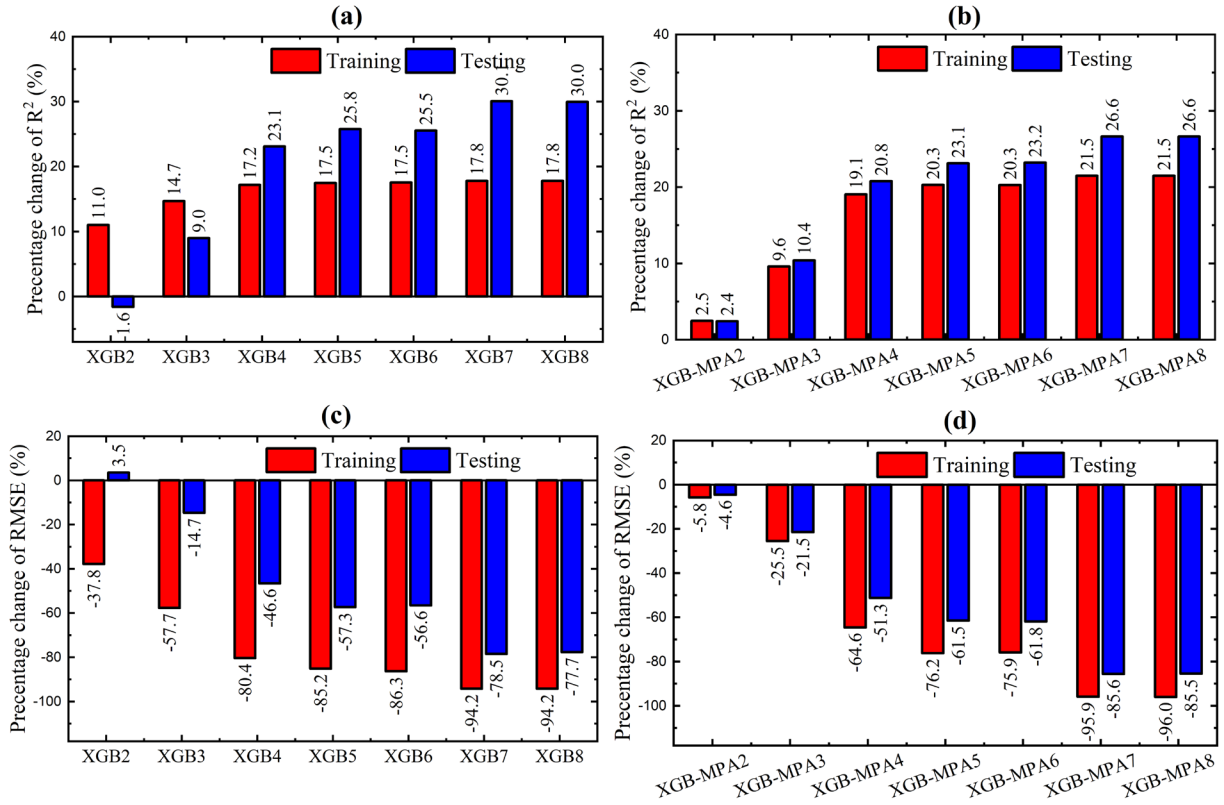

Figure 10. Percentage changes of R^2 (a and b) and RMSE (c and d) based on the first scenario (XGB1 and XGB-MPA1)

In addition, using XGB independently, without any optimization algorithm for hyperparameter tuning, has several disadvantages, including: (*i*) XGB has several hyperparameters that need to be set before training the model, such as the learning rate, maximum depth of trees, number of trees, regularization parameters, and more. Manually tuning these hyperparameters can be a time-consuming and iterative process. It requires domain knowledge, experience, and multiple trial-and-error iterations to find the optimal combination. (*ii*) Suboptimal performance: without proper hyperparameter optimization, the performance of XGB may not reach its full potential. Suboptimal hyperparameter settings can result in a model that underfits or overfits the data, leading to poor generalization on unseen samples. This can result in lower accuracy, higher bias,

548 or higher variance in the model's predictions. By contrast, using an optimization algorithm like
549 MPA for hyperparameter optimization can help mitigate these disadvantages. MPA and similar
550 approaches utilize optimization techniques and search algorithms to automatically explore the
551 hyperparameter space and find the optimal combination of hyperparameters for XGB. This can
552 lead to improved performance, reduced overfitting, and better generalization on unseen data.

553 To further strengthen this study, we compared the performance of the MPA algorithm with PSO
554 in hyperparameter tuning of the XGB algorithm. For each model, twenty independent runs were
555 performed, and the average of the results was reported. For the PSO and MPA algorithm, the
556 population size was set to 50, and the maximum number of train epochs was set to 10. Moreover,
557 the training time of each algorithm is presented in Table 7. As can be seen, the XGB-MPA
558 model has less training time compared to the XGB-PSO model in all scenarios. Moreover, the
559 XGB-MPA outperformed XGB-PSO in all experiments.

560 **Table 7.** Comparison of the XGB-MPA and XGB-PSO models

Model	R^2 (Test)	RMSE (Test)	Training Time (s)
XGB-MPA1	0.7864	1.1931	57.82
XGB-PSO1	0.7858	1.1953	70.58
XGB-MPA2	0.8054	1.1384	87.46
XGB-PSO2	0.8048	1.1401	89.50
XGB-MPA3	0.8682	0.9367	93.11
XGB-PSO3	0.8668	0.9414	98.63
XGB-MPA4	0.9496	0.5815	96.18
XGB-PSO4	0.9490	0.5864	108.18
XGB-MPA5	0.9682	0.4598	120.12
XGB-PSO5	0.9675	0.4653	125.53
XGB-MPA6	0.9689	0.4552	121.90
XGB-PSO6	0.9680	0.4618	135.82
XGB-MPA7	0.9958	0.1713	148.14
XGB-PSO7	0.9954	0.1780	149.82
XGB-MPA8	0.9957	0.1734	145.84

XGB-PSO8	0.9955	0.1776	172.64

4. Discussion

The development of accurate ET_0 prediction models remains a critical challenge in water resource management, particularly in arid regions like Northern Algeria, where efficient irrigation scheduling and water infrastructure planning are paramount. While traditional empirical models have been widely used, they often fall short in capturing the complex interactions between meteorological variables in arid climates, creating a pressing need for more sophisticated modeling approaches. This research addresses several gaps in the current literature, including the limited application of hybrid ML approaches in ET_0 modeling, insufficient validation of modern computational methods in arid regions, and the lack of comprehensive interpretability in advanced prediction models. The current study, while showcasing the potential of XGB coupled with the MPA for ET_0 estimation in northern Algeria, faces several important limitations. The temporal scope of our dataset (2000-2010) may not fully capture recent climate change impacts on ET_0 patterns. In our pursuit of building an accurate model, we employed specific meteorological variables, but overlooked others that might hold significance, such as wind direction, soil moisture, and albedo. Additionally, the computational intensity of the XGB-MPA hybrid approach, while justified by its improved accuracy, may present challenges for real-time applications or resource-limited settings. The intricate interactions with climatic conditions and the scarcity of reliable ET_0 data affect ET_0 modeling in Algeria. In the case of Algeria, where most sites' meteorological datasets are either completely absent or inaccessible because of technical difficulties, this becomes important. In this situation, it should be examined further to ascertain ET_0 for those sites that take into account adjacent locations or pooled data.

The implications of this study extend well beyond the northern Algerian context, offering valuable insights for ET_0 estimation across diverse geographical and climatic conditions. The model's demonstrated ability to handle multiple input combinations makes it particularly adaptable to different data availability scenarios - from data-rich environments where all meteorological variables are available, to data-scarce regions where only basic parameters can be measured. In arid and semi-arid regions similar to our study area, such as parts of the Mediterranean basin, Middle East, and North Africa, the model could be directly applicable with minimal modifications. For regions with different climatic characteristics, such as tropical or temperate zones, the model's flexible architecture allows for recalibration of the MPA optimization parameters and adjustment of the XGB hyperparameters to account for local meteorological patterns. The SHAP-based interpretability approach provides a systematic framework for understanding variable importance in different climatic contexts, potentially helping identify region-specific drivers of ET_0. This adaptability is particularly relevant for developing countries facing similar challenges in water resource management, where the trade-off between model complexity and data availability often constrains the application of sophisticated ET_0 estimation techniques. Furthermore, the model's demonstrated improvement in accuracy with increased input variables suggests it could be particularly valuable in regions transitioning from basic to more comprehensive meteorological monitoring systems.

Based on our findings and identified limitations, several promising directions for future research emerge. First, investigating the model's transferability across diverse climatic zones and testing its performance with different temporal resolutions (hourly, monthly) would enhance its broader applicability. Second, incorporating advanced data preprocessing techniques, such as wavelet transformation or empirical mode decomposition, could potentially improve the model's ability

to capture non-linear patterns in ET_0 dynamics. Third, developing an ensemble framework that combines multiple optimization algorithms could potentially enhance model robustness and reliability. Fourth, investigating the model's performance under future climate scenarios using downscaled climate projections would make the approach more valuable for long-term water resource planning.

5. Conclusions

This study demonstrates that combining XGB with the Marine Predators Algorithm offers a powerful and practical solution for estimating daily evapotranspiration, particularly valuable for regions with limited weather data. Our hybrid model achieved exceptional accuracy (R^2 = 0.9958, RMSE = 0.1713 mm/day) in northern Algeria, significantly outperforming traditional approaches. The analysis revealed that maximum daily temperature, solar radiation, and wind speed were the most influential factors in predicting evapotranspiration, while relative humidity had less impact than conventionally assumed. The model's ability to maintain high accuracy with varying levels of input data makes it particularly suitable for developing regions where comprehensive weather measurements may not be available. Notably, the processing time improvements over existing methods and the model's consistent performance across different weather conditions suggest its potential for practical, real-time applications in water resource management.

While these results are promising, several considerations warrant attention for future applications and research. Although the model proved highly effective in northern Algeria's semi-arid climate, its performance in other climatic zones requires further validation. The current

implementation could benefit from incorporating additional environmental factors such as soil characteristics and landscape features, particularly for regions with diverse topography. Future research should focus on testing the model's adaptability across different geographical and climatic conditions, developing more user-friendly interfaces for practical applications, and exploring the integration of remote sensing data to enhance coverage in data-scarce regions. Despite these limitations, our findings suggest that this hybrid approach offers a reliable tool for irrigation planning and water resource management, particularly valuable for regions facing water scarcity challenges. The model's success demonstrates the potential of combining advanced machine learning techniques with optimization algorithms to address real-world water management challenges. Future research should consider evaluating XGB against other advanced algorithms such as Random Forest, Support Vector Regression, and Long Short-Term Memory networks for ET_0 estimation. Also, future studies can explore the integration of automated feature selection techniques with XGB-MPA to develop more efficient yet robust ET_0 estimation models for different data availability scenarios.

CRediT:

Mohammed Achite: Conceptualization, Formal analysis, Data Curation, Writing - Original Draft, Project administration; **Hamid Nasiri**: Investigation, Methodology, Software, Formal analysis, Writing - Original Draft, Visualization; **Okan Mert Katipoğlu**: Investigation, Writing - Original Draft; **Mohammed Abdallah**: Software, Investigation, Writing - Original Draft, Visualization; **Roozbeh Moazenzadeh**: Methodology, Formal analysis, Validation, Writing - Review & Editing; **Babak Mohammadi**: Conceptualization, Investigation, Methodology,

Software, Validation, Data Curation, Formal analysis, Resources, Writing - Original Draft, Writing - Review & Editing.

Acknowledgments: The authors thank the National Agency of the Water Resources (**ANRH**) for the collected data and the General Directorate of Scientific Research and Technological Development of Algeria (**DGRSDT**).

Funding: This research received no external funding.

Data Availability: Data will be made available on request.

Declarations

Conflict of interest: The authors declare that there is no conflict of interest regarding the publication of this paper.

Ethical approval: This article does not contain any studies with human participants or animals performed by any of the authors.

Appendix:

Appendix A. Time series graphs of observed and estimated ET_0 via XGB and XGB-MPA models (during test sections)

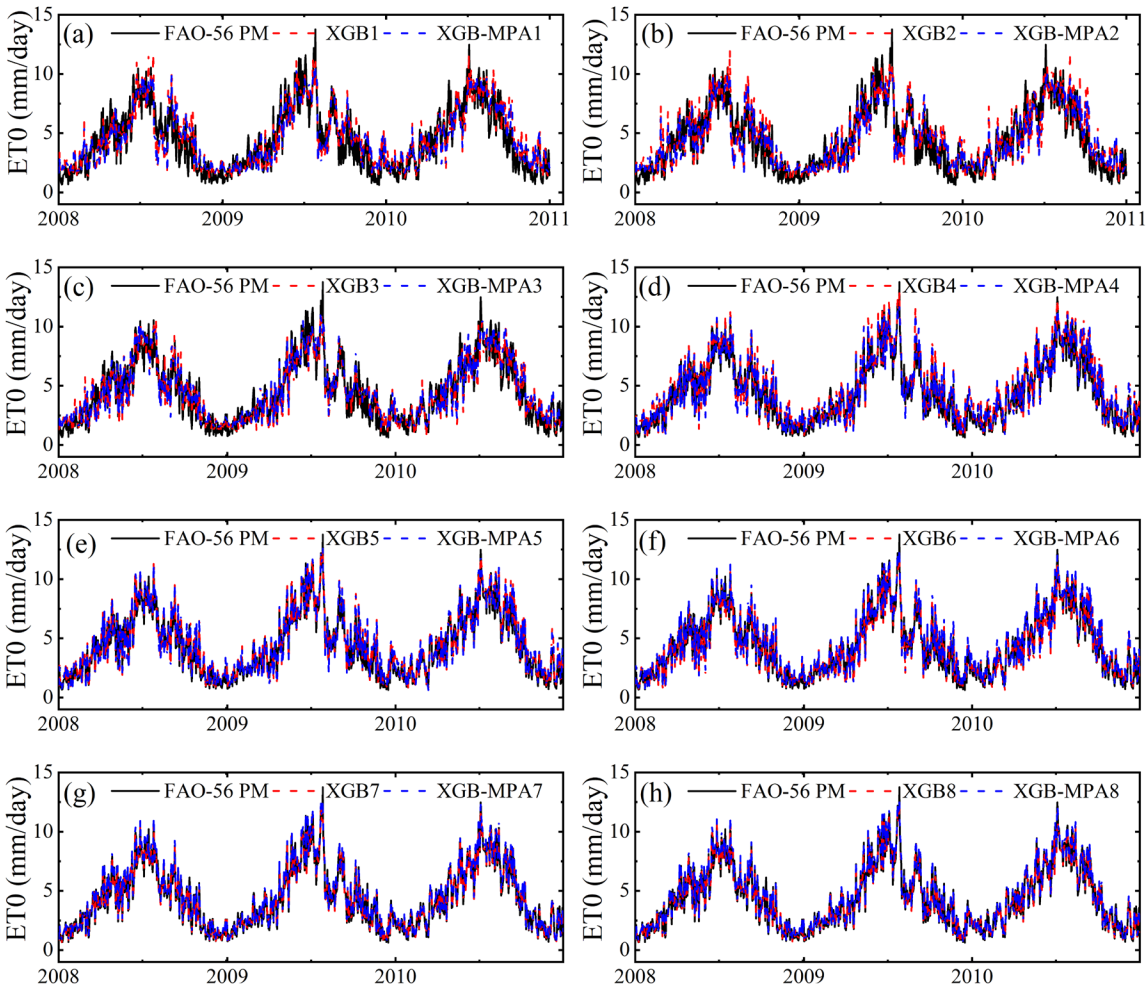

669

670

671 **References**

672 Abd Elminaam DS, Nabil A, Ibraheem SA, Houssein EH (2021): An efficient marine predators algorithm
673 for feature selection. IEEE Access 9, 60136-60153. DOI:10.1109/ACCESS.2021.3073261

674 Abdallah M, Mohammadi B, Zaroug MAH, Omer A, Cheraghalizadeh M, Eldow MEE, Duan Z (2022):
675 Reference evapotranspiration estimation in hyper-arid regions via D-vine copula based-quantile
676 regression and comparison with empirical approaches and machine learning models. J. Hydrol.-
677 Reg. Stud. 44, 26. DOI:10.1016/j.ejrh.2022.101259

678 Abdel-Basset M, Mohamed R, Mirjalili S, Chakrabortty RK, Ryan M (2021): An efficient marine
679 predators algorithm for solving multi-objective optimization problems: analysis and validations.
680 IEEE Access 9, 42817-42844. DOI:10.1109/ACCESS.2021.3066323

681 Abdullah SS, Malek MA, Abdullah NS, Kisi O, Yap KS (2015): Extreme Learning Machines: A new
682 approach for prediction of reference evapotranspiration. J. Hydrol. 527, 184-195.
683 DOI:10.1016/j.jhydrol.2015.04.073

684 Achite M, Jehanzaib M, Sattari MT, Toubal AK, Elshaboury N, Walega A, Krakauer N, Yoo JY, Kim
685 TW (2022): Modern Techniques to Modeling Reference Evapotranspiration in a Semiarid Area
686 Based on ANN and GEP Models. Water 14, 19. DOI:10.3390/w14081210

687 Adnan RM, Heddam S, Yaseen ZM, Shahid S, Kisi O, Li BQ (2021): Prediction of Potential
688 Evapotranspiration Using Temperature-Based Heuristic Approaches. Sustainability 13, 21.
689 DOI:10.3390/su13010297

690 Agrawal Y, Kumar M, Ananthakrishnan S, Kumarapuram G (2022): Evapotranspiration Modeling Using
691 Different Tree Based Ensembled Machine Learning Algorithm. Water Resour. Manag. 36, 1025-
692 1042. DOI:10.1007/s11269-022-03067-7

693 Al-Betar MA, Awadallah MA, Makhadmeh SN, Alyasseri ZAA, Al-Naymat G, Mirjalili S (2023):
694 Marine Predators Algorithm: A Review. Archives of Computational Methods in Engineering, 1-
695 31. DOI:10.1007/s11831-023-09912-1

696 Alizamir M, Kisi O, Adnan RM, Kuriqi A (2020): Modelling reference evapotranspiration by combining
697 neuro-fuzzy and evolutionary strategies. Acta Geophys. 68, 1113-1126. DOI:10.1007/s11600-
698 020-00446-9

699 Allen RG, Smith M, Pereira LS, Raes D, Wright JL (2000): Revised FAO procedures for calculating
700 evapotranspiration: irrigation and drainage paper no. 56 with testing in Idaho, Watershed
701 Management and Operations Management 2000, pp. 1-10

702 Azzam A, Zhang W, Xu C, Khan Z (2023): Calibration and evaluation of Hargreaves-Samani equation
703 for estimating reference evapotranspiration: A case study in the Amu Darya River Basin, Central
704 Asia. Journal of Hydrology: Regional Studies 45, 101298. DOI:10.1016/j.ejrh.2022.101298

Begam B, Bathri D, Charavanan V (2023): Machine Learning-Based Epileptic Seizure Detection Using XGboost Algorithm, 2023 International Conference on Recent Advances in Electrical, Electronics, Ubiquitous Communication, and Computational Intelligence (RAEEUCCI). IEEE, pp. 1-5

Bellido-Jimenez JA, Estevez J, Garcia-Marin AP (2021): New machine learning approaches to improve reference evapotranspiration estimates using intra-daily temperature-based variables in a semi-arid region of Spain. Agric. Water Manage. 245, 16. DOI:10.1016/j.agwat.2020.106558

Bhati BS, Chugh G, Al-Turjman F, Bhati NS (2021): An improved ensemble based intrusion detection technique using XGBoost. Transactions on emerging telecommunications technologies 32, e4076.

Blaney HF (1952): Determining water requirements in irrigated areas from climatological and irrigation data.

Chelgani SC, Nasiri H, Tohry A, Heidari HR (2023): Modeling industrial hydrocyclone operational variables by SHAP-CatBoost-A “conscious lab” approach. Powder Technology 420, 118416.

Chen TQ, Guestrin C, Assoc Comp M (2016): XGBoost: A Scalable Tree Boosting System, 22nd ACM SIGKDD International Conference on Knowledge Discovery and Data Mining (KDD). Assoc Computing Machinery, San Francisco, CA, pp. 785-794

Chen ZJ, Zhu ZC, Jiang H, Sun SJ (2020): Estimating daily reference evapotranspiration based on limited meteorological data using deep learning and classical machine learning methods. J. Hydrol. 591, 12. DOI:10.1016/j.jhydrol.2020.125286

Chetioui, C., Bouregaa, T. (2024). Temperature and precipitation projections from CMIP6 for the Setif high plains in Northeast Algeria. Arabian Journal of Geosciences, 17(2), 63.

Cordova M, Carrillo-Rojas G, Crespo P, Wilcox BP, Celleri R (2015): Evaluation of the Penman-Monteith (FAO 56 PM) Method for Calculating Reference Evapotranspiration Using Limited Data Application to the Wet Paramo of Southern Ecuador. Mt. Res. Dev. 35, 230-239. DOI:10.1659/mrd-journal-d-14-0024.1

e Lucas PdO, Alves MA, e Silva PCdL, Guimaraes FG (2020): Reference evapotranspiration time series forecasting with ensemble of convolutional neural networks. Comput. Electron. Agric. 177, 105700. DOI:10.1016/j.compag.2020.105700

733 Espadafor M, Lorite IJ, Gavilan P, Berengena J (2011): An analysis of the tendency of reference
734 evapotranspiration estimates and other climate variables during the last 45 years in Southern
735 Spain. Agric. Water Manage. 98, 1045-1061. DOI:10.1016/j.agwat.2011.01.015

736 Ewees AA, Ismail FH, Ghoniem RM, Gaheen MA (2022): Enhanced Marine Predators Algorithm for
737 Solving Global Optimization and Feature Selection Problems. Mathematics 10, 4154.

738 Fan JL, Yue WJ, Wu LF, Zhang FC, Cai HJ, Wang XK, Lu XH, Xiang YZ (2018): Evaluation of SVM,
739 ELM and four tree-based ensemble models for predicting daily reference evapotranspiration
740 using limited meteorological data in different climates of China. Agric. For. Meteorol. 263, 225-
741 241. DOI:10.1016/j.agrformet.2018.08.019

742 Fan JL, Ma X, Wu LF, Zhang FC, Yu X, Zeng WZ (2019): Light Gradient Boosting Machine: An
743 efficient soft computing model for estimating daily reference evapotranspiration with local and
744 external meteorological data. Agric. Water Manage. 225, 15. DOI:10.1016/j.agwat.2019.105758

745 Fan JL, Zheng J, Wu LF, Zhang FC (2021): Estimation of daily maize transpiration using support vector
746 machines, extreme gradient boosting, artificial and deep neural networks models. Agric. Water
747 Manage. 245, 12. DOI:10.1016/j.agwat.2020.106547

748 Faramarzi A, Heidarinejad M, Mirjalili S, Gandomi AH (2020): Marine Predators Algorithm: A nature-
749 inspired metaheuristic. Expert systems with applications 152, 113377.
750 DOI:10.1016/j.eswa.2020.113377

751 Fatahi R, Nasiri H, Homafar A, Khosravi R, Siavoshi H, Chehreh Chelgani S (2022): Modeling
752 operational cement rotary kiln variables with explainable artificial intelligence methods–a
753 “conscious lab” development. Particulate Science and Technology, 1-10.

754 Feng Y, Cui NB, Zhao L, Hu XT, Gong DZ (2016): Comparison of ELM, GANN, WNN and empirical
755 models for estimating reference evapotranspiration in humid region of Southwest China. J.
756 Hydrol. 536, 376-383. DOI:10.1016/j.jhydrol.2016.02.053

757 Feng Y, Cui NB, Gong DZ, Zhang QW, Zhao L (2017a): Evaluation of random forests and generalized
758 regression neural networks for daily reference evapotranspiration modelling. Agric. Water
759 Manage. 193, 163-173. DOI:10.1016/j.agwat.2017.08.003

760 Feng Y, Peng Y, Cui NB, Gong DZ, Zhang KD (2017b): Modeling reference evapotranspiration using
761 extreme learning machine and generalized regression neural network only with temperature data.
762 Comput. Electron. Agric. 136, 71-78. DOI:10.1016/j.compag.2017.01.027

763 Ferreira LB, da Cunha FF, de Oliveira RA, Fernandes EI (2019): Estimation of reference
764 evapotranspiration in Brazil with limited meteorological data using ANN and SVM - A new
765 approach. J. Hydrol. 572, 556-570. DOI:10.1016/j.jhydrol.2019.03.028

766 Ferreira LB, da Cunha FF (2020): New approach to estimate daily reference evapotranspiration based on
767 hourly temperature and relative humidity using machine learning and deep learning. Agric. Water
768 Manage. 234, 13. DOI:10.1016/j.agwat.2020.106113

769 Gao LL, Gong DZ, Cui NB, Lv M, Feng Y (2021): Evaluation of bio-inspired optimization algorithms
770 hybrid with artificial neural network for reference crop evapotranspiration estimation. Comput.
771 Electron. Agric. 190, 11. DOI:10.1016/j.compag.2021.106466

772 Gocic M, Petkovic D, Shamshirband S, Kamsin A (2016): Comparative analysis of reference
773 evapotranspiration equations modelling by extreme learning machine. Comput. Electron. Agric.
774 127, 56-63. DOI:10.1016/j.compag.2016.05.017

775 Hadria R, Benabdelouhab T, Lionboui H, Salhi A (2021): Comparative assessment of different reference
776 evapotranspiration models towards a fit calibration for arid and semi-arid areas. J. Arid. Environ.
777 184, 10. DOI:10.1016/j.jaridenv.2020.104318

778 Han YX, Wu JP, Zhai BN, Pan YX, Huang GM, Wu LF, Zeng WZ (2019): Coupling a Bat Algorithm
779 with XGBoost to Estimate Reference Evapotranspiration in the Arid and Semiarid Regions of
780 China. Adv. Meteorol. 2019, 16. DOI:10.1155/2019/9575782

781 Hargreaves GH, Samani ZA (1985): Reference crop evapotranspiration from temperature. Applied
782 engineering in agriculture 1, 96-99. DOI:10.13031/2013.26773

783 Heuillet A, Couthouis F, Díaz-Rodríguez N (2022): Collective explainable AI: Explaining cooperative
784 strategies and agent contribution in multiagent reinforcement learning with shapley values. IEEE
785 Computational Intelligence Magazine 17, 59-71.

786 Huang GM, Wu LF, Ma X, Zhang WQ, Fan JL, Yu X, Zeng WZ, Zhou HM (2019): Evaluation of
787 CatBoost method for prediction of reference evapotranspiration in humid regions. J. Hydrol. 574,
788 1029-1041. DOI:10.1016/j.jhydrol.2019.04.085

789 Ikram RMA, Ewees AA, Parmar KS, Yaseen ZM, Shahid S, Kisi O (2022): The viability of extended
790 marine predators algorithm-based artificial neural networks for streamflow prediction. Appl. Soft.
791 Comput. 131, 17. DOI:10.1016/j.asoc.2022.109739

792 Jayashree TR, Reddy NVS, Acharya UD (2023): Modeling Daily Reference Evapotranspiration from
793 Climate Variables: Assessment of Bagging and Boosting Regression Approaches. Water Resour.
794 Manag. 37, 1013-1032. DOI:10.1007/s11269-022-03399-4

795 Jia Y, Jin SG, Savi P, Gao Y, Tang J, Chen YX, Li WM (2019): GNSS-R Soil Moisture Retrieval Based
796 on a XGboost Machine Learning Aided Method: Performance and Validation. Remote Sens. 11,
797 25. DOI:10.3390/rs11141655

798 Jiang SZ, Liang C, Cui NB, Zhao L, Liu CW, Feng Y, Hu XT, Gong DZ, Zou QY (2020): Water use
799 efficiency and its drivers in four typical agroecosystems based on flux tower measurements.
800 Agric. For. Meteorol. 295, 15. DOI:10.1016/j.agrformet.2020.108200

801 Jing W, Yaseen ZM, Shahid S, Saggi MK, Tao H, Kisi O, Salih SQ, Al-Ansari N, Chau KW (2019):
802 Implementation of evolutionary computing models for reference evapotranspiration modeling:
803 short review, assessment and possible future research directions. Eng. Appl. Comp. Fluid Mech.
804 13, 811-823. DOI:10.1080/19942060.2019.1645045

805 Kennedy, J. and Eberhart, R. (1995): November. Particle swarm optimization. In Proceedings of
806 ICNN'95-international conference on neural networks (Vol. 4, pp. 1942-1948). ieee.

807 Keshtegar B, Kisi O, Arab HG, Zounemat-Kermani M (2018): Subset Modeling Basis ANFIS for
808 Prediction of the Reference Evapotranspiration. Water Resour. Manag. 32, 1101-1116.
809 DOI:10.1007/s11269-017-1857-5

810 Ladlani I, Houichi L, Djemili L, Heddam S, Belouz K (2012): Modeling daily reference
811 evapotranspiration (ET0) in the north of Algeria using generalized regression neural networks
812 (GRNN) and radial basis function neural networks (RBFNN): a comparative study. Meteorol.
813 Atmos. Phys. 118, 163-178. DOI:10.1007/s00703-012-0205-9

Liang S, Pan Y, Zhang H, Zhang J, Wang F, Chen Z (2022): Marine Predators Algorithm Based on Adaptive Weight and Chaos Factor and Its Application. Scientific Programming 2022.

Lundberg SM, Lee S-I (2017): A unified approach to interpreting model predictions. Advances in neural information processing systems 30.

Makkink GF (1957): Testing the Penman formula by means of lysimeters. Journal of the Institution of Water Engineerrs 11, 277-288.

Maroufpoor S, Bozorg-Haddad O, Maroufpoor E (2020): Reference evapotranspiration estimating based on optimal input combination and hybrid artificial intelligent model: Hybridization of artificial neural network with grey wolf optimizer algorithm. J. Hydrol. 588, 125060. DOI:10.1016/j.jhydrol.2020.125060

Mehdizadeh S, Saadatnejadgharahassanlou H, Behmanesh J (2017): Calibration of Hargreaves-Samani and Priestley-Taylor equations in estimating reference evapotranspiration in the Northwest of Iran. Arch. Agron. Soil Sci. 63, 942-955. DOI:10.1080/03650340.2016.1249474

Moazenzadeh R, Izady A (2022): A hybrid calibration method for improving hydrological systems using ground-based and remotely-sensed observations. J. Hydrol. 615, 128688. DOI:10.1016/j.jhydrol.2022.128688

Mohammadi B, Mehdizadeh S (2020): Modeling daily reference evapotranspiration via a novel approach based on support vector regression coupled with whale optimization algorithm. Agric. Water Manage. 237, 14. DOI:10.1016/j.agwat.2020.106145

Mohammadi B, Moazenzadeh R (2021): Performance analysis of daily global solar radiation models in Peru by regression analysis. Atmosphere 12, 389. DOI:10.3390/atmos12030389

Murorunkwere BF, Ihirwe JF, Kayijuka I, Nzabanita J, Haughton D (2023): Comparison of Tree-Based Machine Learning Algorithms to Predict Reporting Behavior of Electronic Billing Machines. Information 14, 140.

Mystakidis S, Davin EL, Gruber N, Seneviratne SI (2016): Constraining future terrestrial carbon cycle projections using observation-based water and carbon flux estimates. Glob. Change Biol. 22, 2198-2215. DOI:10.1111/gcb.13217

841 Nasiri, H. and Ebadzadeh, M.M. (2022) MFRFNN: Multi-functional recurrent fuzzy neural network for
842 chaotic time series prediction. Neurocomputing, 507, 292-310.

843 Nourani V, Elkiran G, Abdullahi J (2019): Multi-station artificial intelligence based ensemble modeling
844 of reference evapotranspiration using pan evaporation measurements. J. Hydrol. 577, 123958.
845 DOI:10.1016/j.jhydrol.2019.123958

846 Oudin L, Hervieu F, Michel C, Perrin C, Andréassian V, Anctil F, Loumagne C (2005): Which potential
847 evapotranspiration input for a lumped rainfall–runoff model?: Part 2—Towards a simple and
848 efficient potential evapotranspiration model for rainfall–runoff modelling. J. Hydrol. 303, 290-
849 306. DOI:10.1016/j.jhydrol.2004.08.026

850 Penman HL (1948): Natural evaporation from open water, bare soil and grass. Proceedings of the Royal
851 Society of London. Series A. Mathematical and Physical Sciences 193, 120-145.
852 DOI:10.1098/rspa.1948.0037

853 Pereira LS, Allen RG, Smith M, Raes D (2015): Crop evapotranspiration estimation with FAO56: Past
854 and future. Agric. Water Manage. 147, 4-20. DOI:10.1016/j.agwat.2014.07.031

855 Priestley CHB, Taylor RJ (1972): On the assessment of surface heat flux and evaporation using large-
856 scale parameters. Monthly weather review 100, 81-92. DOI:https://doi.org/10.1175/1520-
857 0493(1972)100<0081:OTAOSH>2.3.CO;2

858 Reis MM, da Silva AJ, Zullo J, Santos LDT, Azevedo AM, Lopes EMG (2019): Empirical and learning
859 machine approaches to estimating reference evapotranspiration based on temperature data.
860 Comput. Electron. Agric. 165, 10. DOI:10.1016/j.compag.2019.104937

861 Rezaie-Balf, M., Kim, S., Ghaemi, A. and Deo, R. (2021): Design and performance of two decomposition
862 paradigms in forecasting daily solar radiation with evolutionary polynomial regression: wavelet
863 transform versus ensemble empirical mode decomposition. In Predictive Modelling for Energy
864 Management and Power Systems Engineering (pp. 115-142). Elsevier.

865 Salam R, Islam AMT (2020): Potential of RT, bagging and RS ensemble learning algorithms for
866 reference evapotranspiration prediction using climatic data-limited humid region in Bangladesh.
867 J. Hydrol. 590, 17. DOI:10.1016/j.jhydrol.2020.125241

868 Sarigol M, Katipoglu OM (2023): Estimation of monthly evaporation values using gradient boosting
869 machines and mode decomposition techniques in the Southeast Anatolia Project (GAP) area in
870 Turkey. Acta Geophys., 18. DOI:10.1007/s11600-023-01067-8

871 Shiri J, Marti P, Nazemi AH, Sadraddini AA, Kisi O, Landeras G, Fard AF (2015): Local vs. external
872 training of neuro-fuzzy and neural networks models for estimating reference evapotranspiration
873 assessed through k-fold testing. Hydrol. Res. 46, 72-88. DOI:10.2166/nh.2013.112

874 Sun, K., Rajabtabar, M., Samadi, S., Rezaie-Balf, M., Ghaemi, A., Band, S. S., & Mosavi, A. (2021): An
875 integrated machine learning, noise suppression, and population-based algorithm to improve total
876 dissolved solids prediction. Engineering Applications of Computational Fluid Mechanics, 15(1),
877 251-271.

878 Sun Y, Huang Q, Liu T, Cheng Y, Li Y (2023): Multi-Strategy Enhanced Harris Hawks Optimization for
879 Global Optimization and Deep Learning-Based Channel Estimation Problems. Mathematics 11,
880 390.

881 Tadlaoui, S. (2018). Assessment of Climate Change and Its Impact on Water Resources: Case of Tafna
882 Basin–North West of Algeria (Master's thesis).

883 Temesgen B, Eching S, Davidoff B, Frame K (2005): Comparison of some reference evapotranspiration
884 equations for California. Journal of irrigation and drainage engineering 131, 73-84.
885 DOI:10.1061/(ASCE)0733-9437(2005)131:1(73

886 Trajkovic S, Kolakovic S (2010): Comparison of simplified pan-based equations for estimating reference
887 evapotranspiration. Journal of irrigation and drainage engineering 136, 137-140.
888 DOI:10.1061/(ASCE)IR.1943-4774.000013

889 Valle LCG, Ventura TM, Gomes RSR, Nogueira JD, Lobo FD, Vourlitis GL, Rodrigues TR (2020):
890 Comparative assessment of modelled and empirical reference evapotranspiration methods for a
891 brazilian savanna. Agric. Water Manage. 232, 13. DOI:10.1016/j.agwat.2020.106040

892 Wang S, Lian JJ, Peng YZ, Hu BQ, Chen HS (2019): Generalized reference evapotranspiration models
893 with limited climatic data based on random forest and gene expression programming in Guangxi,
894 China. Agric. Water Manage. 221, 220-230. DOI:10.1016/j.agwat.2019.03.027

Xu SQ, Yu ZB, Yang CG, Ji XB, Zhang K (2018): Trends in evapotranspiration and their responses to climate change and vegetation greening over the upper reaches of the Yellow River Basin. Agric. For. Meteorol. 263, 118-129. DOI:10.1016/j.agrformet.2018.08.010

Yamac SS, Todorovic M (2020): Estimation of daily potato crop evapotranspiration using three different machine learning algorithms and four scenarios of available meteorological data. Agric. Water Manage. 228, 12. DOI:10.1016/j.agwat.2019.105875

Yan SC, Wu LF, Fan JL, Zhang FC, Zou YF, Wu Y (2021): A novel hybrid WOA-XGB model for estimating daily reference evapotranspiration using local and external meteorological data: Applications in arid and humid regions of China. Agric. Water Manage. 244, 22. DOI:10.1016/j.agwat.2020.106594

Yang Y, Chen RS, Han CT, Liu ZW (2021): Evaluation of 18 models for calculating potential evapotranspiration in different climatic zones of China. Agric. Water Manage. 244, 19. DOI:10.1016/j.agwat.2020.106545

Yassin MA, Alazba AA, Mattar MA (2016): Artificial neural networks versus gene expression programming for estimating reference evapotranspiration in arid climate. Agric. Water Manage. 163, 110-124. DOI:10.1016/j.agwat.2015.09.009

Yu JX, Zheng WG, Xu LL, Zhangzhong LL, Zhang G, Shan FF (2020): A PSO-XGBoost Model for Estimating Daily Reference Evapotranspiration in the Solar Greenhouse. Intell. Autom. Soft Comput. 26, 989-1003. DOI:10.32604/iasc.2020.010130

Zhao, N., Ghaemi, A., Wu, C., Band, S. S., Chau, K. W., Zaguia, A., ... & Mosavi, A. H. (2021): A decomposition and multi-objective evolutionary optimization model for suspended sediment load prediction in rivers. Engineering Applications of Computational Fluid Mechanics, 15(1), 1811-1829.

Zhang J, Ma X, Zhang J, Sun D, Zhou X, Mi C, Wen H (2023): Insights into geospatial heterogeneity of landslide susceptibility based on the SHAP-XGBoost model. Journal of Environmental Management 332, 117357.

Zhang ZX, Gong YC, Wang ZJ (2018): Accessible remote sensing data based reference evapotranspiration estimation modelling. Agric. Water Manage. 210, 59-69. DOI:10.1016/j.agwat.2018.07.039

924 Zhao TTG, Wang QJ, Schepen A, Griffiths M (2019): Ensemble forecasting of monthly and seasonal
925 reference crop evapotranspiration based on global climate model outputs. Agric. For. Meteorol.
926 264, 114-124. DOI:10.1016/j.agrformet.2018.10.001

927 Zhu B, Feng Y, Gong DZ, Jiang SZ, Zhao L, Cui NB (2020): Hybrid particle swarm optimization with
928 extreme learning machine for daily reference evapotranspiration prediction from limited climatic
929 data. Comput. Electron. Agric. 173, 13. DOI:10.1016/j.compag.2020.105430

930